Anders Olsson

Fabrication and Characterization of Thermophotonic Devices

Faculty of Electronics, Communications and Automation

Thesis submitted for examination for the degree of Master of Science in Technology.

Espoo 19.5.2011

Thesis supervisor:

Prof. Jukka Tulkki

Thesis instructor:

D.Sc. (Tech.) Jani Oksanen

Aalto University
School of Science
and Technology

AALTO-YLIOPISTO
TEKNILLINEN KORKEAKOULU

DIPLOMITYÖN
TIIVISTELMÄ

Tekijä: Anders Olsson

Työn nimi: Termofotonisten laitteiden valmistus ja karakterisointi

Päivämäärä: 19.5.2011 Kieli: Englanti Sivumäärä:9+46

Elektroniikan, tietoliikenteen ja automaation tiedekunta

Lääketieteellisen tekniikan ja laskennallisen tieteen laitos

Professuuri: Biologinen tekniikka Koodi: S3002

Valvoja: Prof. Jukka Tulkki

Ohjaaja: TkT Jani Oksanen

Tässä diplomityössä tutkitaan termofotonisille laitteille tarkoitettujen LED-rakenteiden valmistusta ja karakterisointia. Termofotonisen laitteen toiminta perustuu elektroluminesenssijäähdytykseen, eli LEDin kykyyn emittoida fotoneja, jotka ovat saanet osan energiastaan hilalämmöstä. Ilmiö saattaa mahdollistaa LEDin jäähtymisen sen emittoidessa valoa, jos häviöt ovat riittävän pieniä. Työn teoreettisessä osassa käsitellään lyhyesti LEDien ja metallikontaktien perusominaisuuksia. Metallikontakteja käytetään injektoimaan virtaa ja heijastamaan valoa rakenteissa. Valmistusprosessi alkaa indiumfosfidi (InP) puolijohdesubstraatista, jonka pinnalle kasvatetaan useita puolijohdekerroksia, ml. aktiivinen InGaAs-kerros, tavoitteena saada aikaan valoa emittoiva p-n-liitos. Sähköiset kontaktit valmistetaan höyrystämällä metallia puolijohderakenteiden pinnalle. Valmistetut rakenteet karakterisoidaan fotoluminesenssimittauksilla (PL), virta-jännitemittauksilla (I-V) ja atomivoimamikroskoopilla (AFM). Näytteitä valmistettiin työn aikana 63 kpl, joista 22 oli valmiita InP/InGaAs p-n-liitos LED-rakenteita joiden PL-huiput sijoittuivat välille 1630-1690 nm.

Avainsanat: Termofotoniikka, LED, lämpöpumppu, elektroluminesenssi, jäähdytys, jäähdytyslaite, indiumfosfidi, indiumgalliumarsenidi.

AALTO UNIVERSITY
SCHOOL OF SCIENCE AND TECHNOLOGY

ABSTRACT OF THE
MASTER'S THESIS

Author: Anders Olsson

Title: Fabrication and Characterization of Thermophotonic Devices

Date: 19.5.2011 Language: English Number of pages:9+46

Faculty of Electronics, Communications and Automation

Department of Biomedical Engineering and Computational Science

Professorship: Bioengineering Code: S3002

Supervisor: Prof. Jukka Tulkki

Instructor: D.Sc. (Tech.) Jani Oksanen

In this thesis, the fabrication properties and characterization of broad area light-emitting LED structures for thermophotonic devices are studied. The operation of a thermophotonic device is based on electroluminescent cooling, i.e. the ability of an LED to emit photons that have received a part of their energy from the lattice heat. This phenomenon allows an LED to cool down as it emits light if other losses are sufficiently small. The theoretical part of the work briefly reviews the basic properties of light-emitting diodes and metal contacts used to inject current and to reflect light in the structures. The fabrication process starts with indium phosphide (InP) semiconductor wafers, on which several semiconductor layers are grown, including an InGaAs active layer, in order to create a p-n junction capable of emitting light. Electrical contacts are made by evaporating metal on the semiconductor structures. The structures fabricated are characterized by photoluminescence (PL) measurements, then by current-voltage (I-V) measurements and also by atomic force microscopy (AFM) which are also briefly reviewed in this work. Of the 63 fabricated samples 22 were complete InP/InGaAs p-n junction LED structures whose PL peaks were in the range 1630-1690 nm.

Keywords: Thermophotonics, LED, heat pump, electroluminescent cooling, cooling device, indium phosphide, indium gallium arsenide.

Preface

I would like to thank Prof. Jukka Tulkki and Dr. Jani Oksanen for supervising my thesis. Thanks also go to all the people working at the various laboratories at the 4th floor of Micronova, especially Dr. Abuduwayiti Aierken for operating the MOVPE system and giving me help when needed. This work has been partly funded by Multidisciplinary Institute of Digitalisation and Energy (MIDE).

Otaniemi, 24.3.2011

Anders Olsson

Contents

Symbols and abbreviations

Symbols

c	speed of light in vacuum
$D_{n,p}$	electron and hole diffusion constants
e	elementary electronic charge
E_C	energy of the conduction band edge
E_V	energy of the valence band edge
E_g	band gap of a semiconductor
E_F	Fermi energy
h	Planck's constant
I	current
I_s	saturation current of a diode
n_i	intrinsic carrier concentration
n_{ideal}	ideality factor of a diode
η_{ext}	external quantum efficiency of an LED
$\eta_{\text{extraction}}$	extraction efficiency of an LED
η_{int}	internal quantum efficiency of an LED
η_{power}	power efficiency of an LED
$N_{D,A}$	donor and acceptor concentrations
$\Phi_{m,s}$	metal and semiconductor work functions
$\tau_{n,p}$	electron and hole minority carrier lifetimes
V_D	internal (diffusion) voltage of a p-n junction
χ_s	electron affinity of a semiconductor

Abbreviations

AFM	Atomic Force Microscope
COP	Coefficient of performance
CVD	Chemical vapor deposition
EBE	Electron beam evaporation
EL	Electroluminescence
ICP	Inductively Coupled Plasma
LED	Light-emitting diode
MOVPE	Metalorganic vapor phase epitaxy
MQW	Multiple quantum well
PL	Photoluminescence
RF	Radio frequency
RIE	Reactive Ion Etching
TE	Thermoelectric
THP	Thermophotonic heat pump
XRD	X-ray diffraction

1 Introduction

The most successful solid state cooling device to this date is the thermoelectric (TE) cooler. The operation of the device is based on the ability of electrons to transport heat as well as electric charge. Commercial TE devices typically have an efficiency of under 10% of the ideal Carnot limit.

It has been shown, that under certain conditions, the energy of the photons emitted by a light-emitting diode (LED) is higher than the electrical energy required to inject the electron-hole pair [1]. This is possible because the photon receives a part of its energy from lattice heat. This phenomenon would allow a LED to cool down as it emits light if other losses are sufficiently small. The phenomenon is called electroluminescent (EL) cooling. EL cooling of LEDs hasn't been experimentally demonstrated to date because the overall losses in conventional LED structures are too high. In other words, too much energy is lost when extracting light from the emitting semiconductor material into air and cooling doesn't take place.

A new cooling device, the thermophotonic heat pump (THP), based on EL cooling has been proposed recently [2]. The THP structure is expected to solve the problems related to light extraction and thereby enable demonstrating EL cooling. The device essentially consists of two optically coupled light-emitting diodes. One of the LEDs of the structure emits light with energy obtained from an external power source and the lattice heat. The other acts as a photovoltaic cell; it absorbs the photons emitted by the emitter and releases the absorbed energy as electricity and heat.

The relative simplicity of the structure of the THP makes it a viable candidate for a new commercial cooling device for electronics; the materials and fabrication techniques required are well known and suitable for mass production. Few fabrication steps are needed compared to other modern semiconductor devices. Simulations have shown that the coefficient of performance (COP) of the device could potentially be very high, allowing high cooling power with low input power [3].

The original aim of this work was the fabrication and characterization of the properties of a prototype of the thermophotonic heat pump. However, because of challenges met in the process of fabrication, a complete prototype of the THP was not produced. Instead, the LEDs of which the THP consists of were fabricated and the properties of these, as well as possible reasons for the challenges arisen in the complete THP fabrication, are discussed.

The fabrication process starts with indium phosphide (InP) semiconductor wafers, on which several semiconductor layers are grown in order to create a p-n junction capable of emitting light. Electrical contacts are made by evaporating metal on the semiconductor structures. The quality and properties of the layered semiconductors are determined with different type of luminescence and IV-curve measurements.

This work starts by a brief introduction to the theory of p-n junctions, LEDs and the THP in Chapter 2. Chapter 3 continues by describing selected key device properties

that have been predicted to essentially affect the performance of the THP. Chapters 4 and 5 present the techniques of fabrication, including metalorganic vapor phase epitaxy and metal evaporation, and types of measurement, e.g. photoluminescence of semiconductors and current-voltage characteristics used in this work. Finally, in Chapter 6, the measurement results of the properties of the fabricated samples are shown and analyzed.

2 Background

2.1 The p-n junction diode

The electrical properties of semiconductors strongly depend on the presence of impurities in the crystal structure. Very pure, i.e. intrinsic, semiconductors are semi-insulating but adding small amounts of impurity atoms makes them extrinsic and can increase the conductivity enormously. For Si and Ge these impurity atoms are typically elements of Column III or Column V in the periodic table. For InP, however, Zn (p-type) an Si (n-type) are used (as is the case in this work). Impurity atoms that can release an electron in the conduction band are called donors, while atoms that can capture one electron from the valence band and thus generate a hole are called acceptors. [4]

When donors are added to the intrinsic semiconductor, free electrons become more abundant (majority carriers) and holes become less abundant (minority carriers). Similarly, when acceptor atoms are added, holes and electrons become majority and minority carriers, respectively. When the electron density is increased the resulting semiconductor is called n-type and when the hole density is increased it is called p-type. Note that extrinsic semiconductors are still charge neutral. [4]

If a p-type semiconductor is joined with an n-type semiconductor they form a p-n junction (Figure 1). The contact between the p- and n-type materials allows holes to diffuse from the p-type material to the n-type material and electrons from the n-type material to the p-type material because of the carrier concentration gradients. Every electron that leaves the n region leaves behind a positively ionized donor impurity atom and every hole that leaves the p region leaves behind a negatively charge acceptor. As a result, the region near the contact surface is called the depletion region, because it is depleted of electrons and holes but contains positive donor atoms and negative acceptor atoms on opposite sides. The n side of the depletion region is positively charged and the p side is negatively charged. The width of the depletion region depends on the structure and doping of the p-n junction. [4]

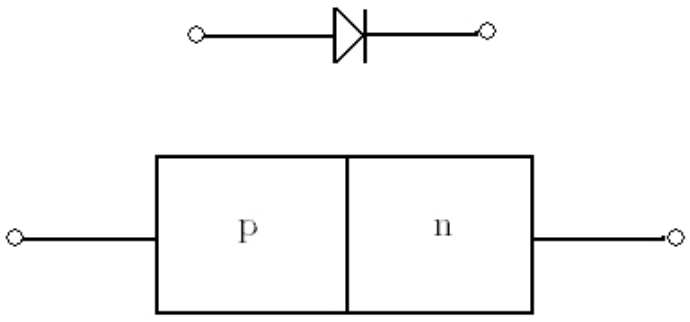

Figure 1: The symbol of a p-n junction diode and a schematic picture of the diode structure.

In crystalline semiconductor solids, electrons reside in energy bands. The relevant bands of semiconductors in which electrons can exist are the conduction band (E_C) and the valence band (E_V). These two bands are separated by a band in which no electrons can exist. The gap is known as the energy gap or band gap but usually these terms refer to the width (E_g) of the gap [5]. At absolute zero temperature, no electrons occupy the conduction band. In semiconductor physics the Fermi level (E_F) is the chemical potential of electrons, which describes the electron distribution in the system. [6].

The charges in the depletion layer cause an electric field directed from the n- to the p-side. The electric field produces a voltage across the depletion region called the internal, or diffusion, voltage V_D. The diffusion voltage is accompanied by the bending of the energy bands of the p-n junction (Figure 2(a)). The consequence of the bending is that an energy equal to $e\,V_D$ is required to move a positive charge from the p-side (at lower potential) to the n-side (at higher potential) against the electric field, where e is the electronic charge.

When a bias voltage is applied across the junction the voltage barrier over the depletion region either decreases (forward bias) or increases (reverse bias). When forward bias V is applied, electrons and holes are injected to the opposite conductivity type regions and the current flow increases. The energy bands are affected by the forward bias and are presented in Figure 2(b).

The current-voltage (I-V) characteristics of a p-n junction diode is described by the Shockley equation and it states that the current through a diode is [7]

$$I = e\,A\left(\frac{n_i^2}{N_D}\sqrt{\frac{D_p}{\tau_p}} + \frac{n_i^2}{N_A}\sqrt{\frac{D_n}{\tau_n}}\right)\left(\mathrm{e}^{eV/kT} - 1\right), \tag{1}$$

where A is the cross-sectional area of the diode, $D_{n,p}$ and $\tau_{n,p}$ are the electron and hole diffusion constants and the electron and hole minority carrier lifetimes, respectively, $N_{D,A}$ are the donor and acceptor concentrations and n_i is the intrinsic carrier concentration of the semiconductor.

Under reverse bias ($V < 0$) the current through the diode saturates to the factor preceding the exponential function in equation (1). Equation (1) can be rewritten as

$$I = I_s\left(\mathrm{e}^{eV/kT} - 1\right), \quad \text{where} \quad I_s = e\,A\left(\frac{n_i^2}{N_D}\sqrt{\frac{D_p}{\tau_p}} + \frac{n_i^2}{N_A}\sqrt{\frac{D_n}{\tau_n}}\right). \tag{2}$$

Under forward bias, typically $V >> kT/e$, and thus $[\exp(e\,V/kT) - 1] \approx \exp(e\,V/kT)$

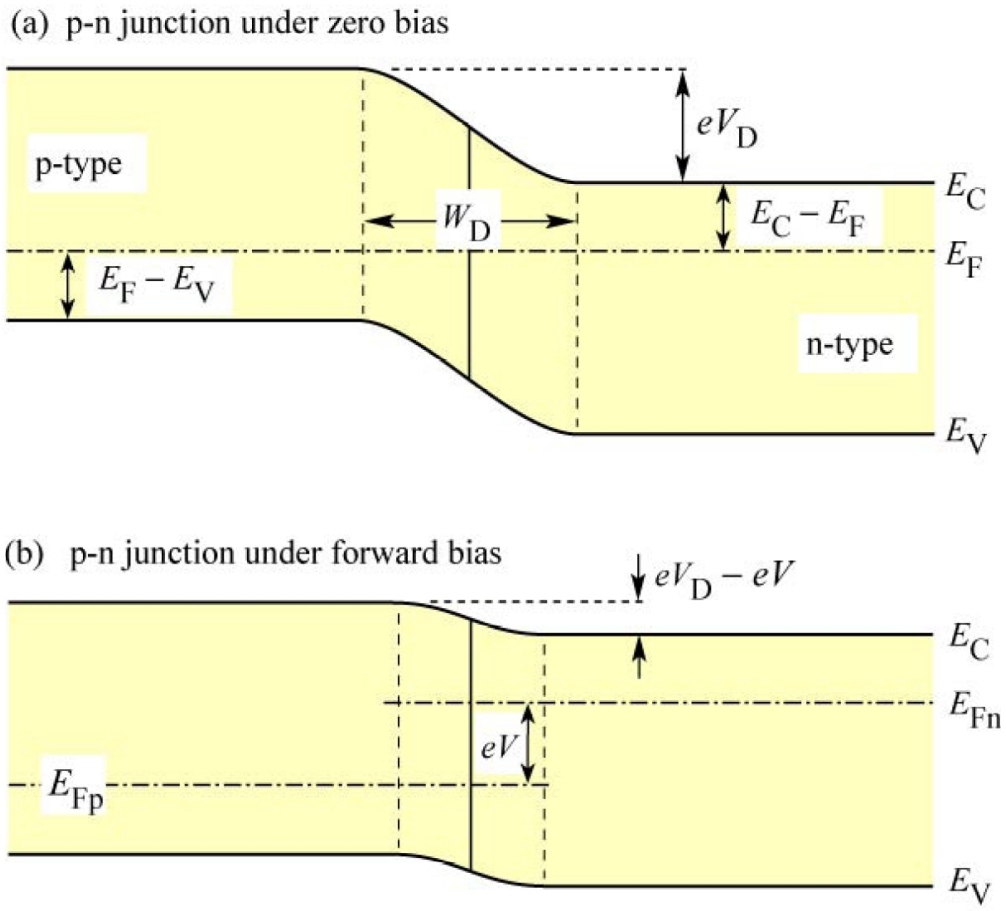

Figure 2: Energy band diagrams for the p-n junction diode under (a) zero bias and (b) forward bias. Under zero bias the diode is in thermal equilibrium and the Fermi level E_F is constant. Forward bias decreases the potential barrier seen by electrons and holes, which allows larger current through the diode and separates the Fermi level into separate quasi-Fermi levels for electrons (E_{Fn}) and holes (E_{Fp}). [8]

which allows the Shockley equation to be written as

$$I = e\,A\left(\frac{n_i^2}{N_D}\sqrt{\frac{D_p}{\tau_p}} + \frac{n_i^2}{N_A}\sqrt{\frac{D_n}{\tau_n}}\right)\mathrm{e}^{eV/kT}. \tag{3}$$

The Shockley equation describes the ideal behavior of a diode. When experimentally measuring diodes, the characteristics are described by

$$I = I_s\,\mathrm{e}^{eV/(n_{\mathrm{ideal}}\,kT)} \quad , \tag{4}$$

where n_{ideal} is the ideality factor of the diode. For a perfect diode $n_{\mathrm{ideal}} = 1$ and Equation (4) reduces to the Shockley equation. For real diodes $n_{\mathrm{ideal}} > 1$ (typically 1.1-1.5).

Frequently a diode has parasitic resistances. A series resistance can arise, for instance, from resistance in the electrical contact to the diode. A parallel resistance can be caused by any route that bypasses the p-n junction, typically the edges of the device or material impurities. Assuming a parallel resistance R_p and a series resistance R_s the Shockley equation can be written as

$$I - \frac{V - I\,R_s}{R_p} = I_s\,\mathrm{e}^{e(V - I\,R_s)/(n_{\mathrm{ideal}}\,kT)}. \tag{5}$$

For $R_p \to \infty$, $R_s = 0$ and $n_{\mathrm{ideal}} = 1$, Equation (5) reduces to the Shockley equation. Writing the voltage over the diode as $V_d = V - I\,R_s$, Equation (5) can be presented more clearly in parametric form:

$$I = I_s\,\mathrm{e}^{e\,V_d/(n_{\mathrm{ideal}}\,kT)} + \frac{V_d}{R_p}. \tag{6}$$

2.2 Light-emitting diode

A light-emitting diode (LED) is a p-n junction that can emit light by spontaneous emission of radiation. Holes flow into the junction from the p-side (anode) and electrons from the n-side (cathode). In the active region an electron recombines with a hole (the electron moves from the conduction band to the valence band) and energy is released in the form of a photon. The wavelength of the emitted light depends on the band gap of the emitting (active) material. [8]

The band gap of a semiconductor is one of two types, a direct band gap or an indirect band gap. If the minimum energy in the conduction band and the maximum energy in the valence band have the same k-vector, the semiconductor is direct band gap, otherwise it is indirect band gap (Figure 3). Direct band gap semiconductors include InP and InGaAs while Si is an example of an indirect band gap semiconductor. When an electron is near the bottom of the conduction band and a hole is near the top of the valence band, they have a high probability of recombining in a direct band gap semiconductor. In an indirect band gap semiconductor, the absorption or emission of a phonon with a momentum equal to the difference in the momentums of the electron and hole must occur in order for radiative recombination to happen. Thus, radiative recombination is much less abundant in indirect band gap semiconductors.

Ideally, an LED emits one photon for every electron injected. In reality, this is not the case and we define the internal quantum efficiency of an LED as

$$\eta_{\mathrm{int}} = \frac{\text{number of photons emitted from active region per second}}{\text{number of electrons injected into LED per second}} = \frac{P_{\mathrm{int}}/(hf)}{I/e}, \tag{7}$$

where P_{int} is the optical power emitted from the active region and I is the injection current.

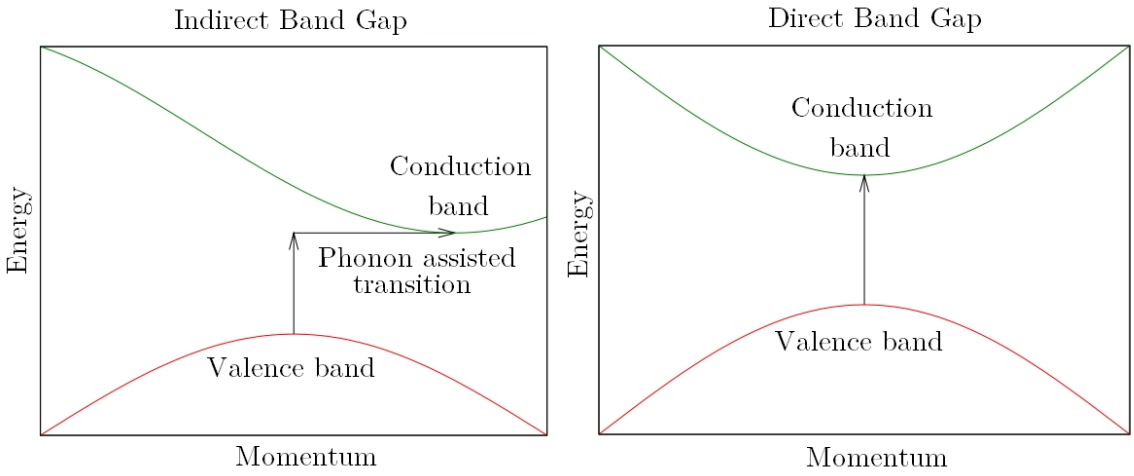

Figure 3: Energy levels of the conduction and valence bands with respect to crystal momentum in direct (left) and indirect (right) band gap semiconductors.

All photons emitted from the active region ideally escape the LED die. In practice, however, photons can be absorbed by the semiconductor material or metal contacts and some light never escapes the semiconductor due to total internal reflection. We define the extraction efficiency of an LED as

$$\eta_{\text{extraction}} = \frac{\text{number of photons emitted into free space per second}}{\text{number of photons emitted from active region per second}} = \frac{P/(hf)}{P_{\text{int}}/(hf)}, \tag{8}$$

where P is the optical power emitted into free space.

The external quantum efficiency is defined as

$$\begin{aligned}\eta_{\text{ext}} &= \frac{\text{number of photons emitted into free space per second}}{\text{number of electrons injected into LED per second}} = \frac{P/(hf)}{I/e} \\ &= \eta_{\text{int}}\,\eta_{\text{extraction}}.\end{aligned} \tag{9}$$

The external quantum efficiency gives the ratio of the number of useful photons to the number of injected charge carriers.

The power efficiency is defined as

$$\eta_{\text{power}} = \frac{P}{IV}, \tag{10}$$

where IV is the electrical power provided to the LED.

It has been shown, that the energy of the photons emitted by an LED can be higher than the electrical energy required to inject the electron-hole pair [1]. This is possible because the photon receives a part of its energy from lattice heat. This phenomenon would allow an LED to cool down as it emits light if other losses are sufficiently small. The phenomenon is called electroluminescent (EL) cooling. In the regime of EL cooling $P > IV$ and thus $\eta_{\text{power}} > 1$ in Equation (10).

Under equilibrium conditions and at a specific temperature, the law of mass action states that the product of the electron and hole concentrations is a constant, i.e.

$$n_0\, p_0 = n_i^2 \quad , \tag{11}$$

where n_0 and p_0 are electron and hole concentrations, respectively and n_i is the intrinsic carrier concentration. When injecting a current or absorbing light, excess carriers are generated in the material and the total carrier concentrations are

$$n = n_0 + \Delta n \quad \text{and} \quad p = p_0 + \Delta p \quad , \tag{12}$$

where Δn and Δp are the excess carrier concentrations.

When an electron combines with a hole, the carriers disappear and a photon is emitted. Considering a free electron in the conduction band, the probability that it radiatively recombines with a hole is proportional to the hole concentration, i.e. for the rate of recombination holds $R \propto p$. Using the same reasoning, the rate of recombination is also proportional to the electron concentration. Thus, the rate of recombination is proportional to the product of the electron and hole concentrations, $R \propto n\, p$. Taking into account the disappearance of charge carriers due to photon emission, the rate of radiative recombination is written as

$$R = -\frac{\mathrm{d}n}{\mathrm{d}t} = -\frac{\mathrm{d}p}{\mathrm{d}t} = B\, n\, p \quad , \tag{13}$$

where B is the proportionality constant called the bimolecular recombination coefficient. Equation (13) is called the bimolecular rate equation.

From Equation (13) we see that an increase in carrier concentrations results in a higher photon emission rate. A double heterostructure allows carriers to be confined in a lower band gap area. The structure consists of a higher band gap n-type material, a higher band gap p-type material and an (often) intrinsic lower band gap material in between (Figure 4). Thus, the junction that is created is a p-i-n junction. The main advantages of the double heterostructure are that the barrier materials are transparent to the light emitted by the active region and the dimensions of the light emitting region can be easily controlled.

In a double heterostructure the confinement layers have a larger band gap than the active layer. If the difference in band gap energies between the confinement (cladding) and active layers is ΔE_g then there are discontinuities in the conduction and valence bands which follow the relation

$$\Delta E_g = E_{g,\text{cladding}} - E_{g,\text{active}} = \Delta E_C + \Delta E_V \quad , \tag{14}$$

where $E_{g,\text{cladding}}$ is the cladding layer band gap, $E_{g,\text{active}}$ is the active layer band gap and ΔE_C and ΔE_V are the differences in the conduction and valence band energies, respectively, between the cladding and active layers. Determining the exact distribution of the discontinuity between the conduction and valence bands is generally challenging. The first estimate for InP based materials is often the 70/30 rule stating that 70 % of the discontinuity is in the conduction band. The effect of a double heterostructure on carrier distributions is presented in Figure 5.

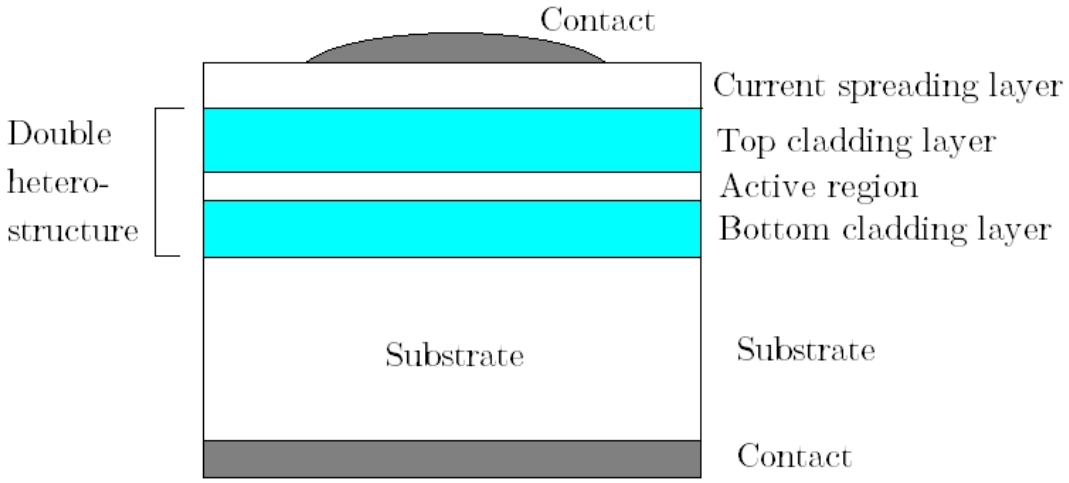

Figure 4: Schematic picture of the double heterostructure LED.

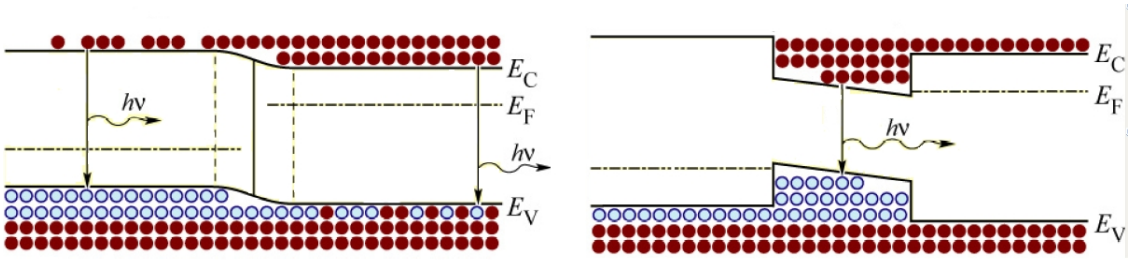

Figure 5: Schematic picture of the carrier distributions in a homojuntion (left) and a double heterostructure (right). In the heterojunction the carriers are confined to the active region. Dark red circles represent electrons in conduction and valence bands and blue circles represent holes, i.e. empty valence band states. [8]

2.3 Thermophotonic heat pump

The most successful solid state heat pump today, is the thermoelectric (TE) cooler. The operation of a TE cooler is based on the ability of an electric current to carry heat alongside electric charge. A drawback is the low efficiency of commercial devices (typically about 10% of the Carnot limit) which is contributed to by the fact that electrically conducting materials also tend to conduct heat and the thermoelectrically transported heat is partly conducted back to the cooled part of the device.

As discussed in section 2.2 EL cooling would allow an LED to cool down by emitting photons whose energies were partly received from the LEDs lattice heat. For GaAs materials very high internal quantum efficiencies have been reported [9]. Also very high quantum efficiencies have been demonstrated for intrinsic structures without metallic contacts [10]. Despite these very high efficiencies, EL cooling has not yet been demonstrated in practice. The main challenges in the first demonstration of EL cooling are expected to be caused by the trapping of light in typical semiconductors having very high quantum efficiency. This trapping effectively amplifies the initially

small losses caused by e.g. the contact metals and non-radiative recombination and prevents EL cooling.

To partly resolve the light trapping problem a new cooling device, the thermophotonic heat pump (THP), based on EL cooling has been proposed in Ref. [2]. The THP could also solve the problem of the TE cooler where the reverse heat flow can not be easily controlled: separation of the heated and cooled side allows them to thermally isolate from one another much more efficiently.

The THP consists of two large area optically coupled light-emitting diodes presented in Figure 6. The LED on the cooled side of the structure emits light with energy obtained from an external power source and the lattice heat. The LED on the heated side acts as a photovoltaic cell; it absorbs the photons emitted by the LED on the cooled side and releases the energy as electricity and heat.

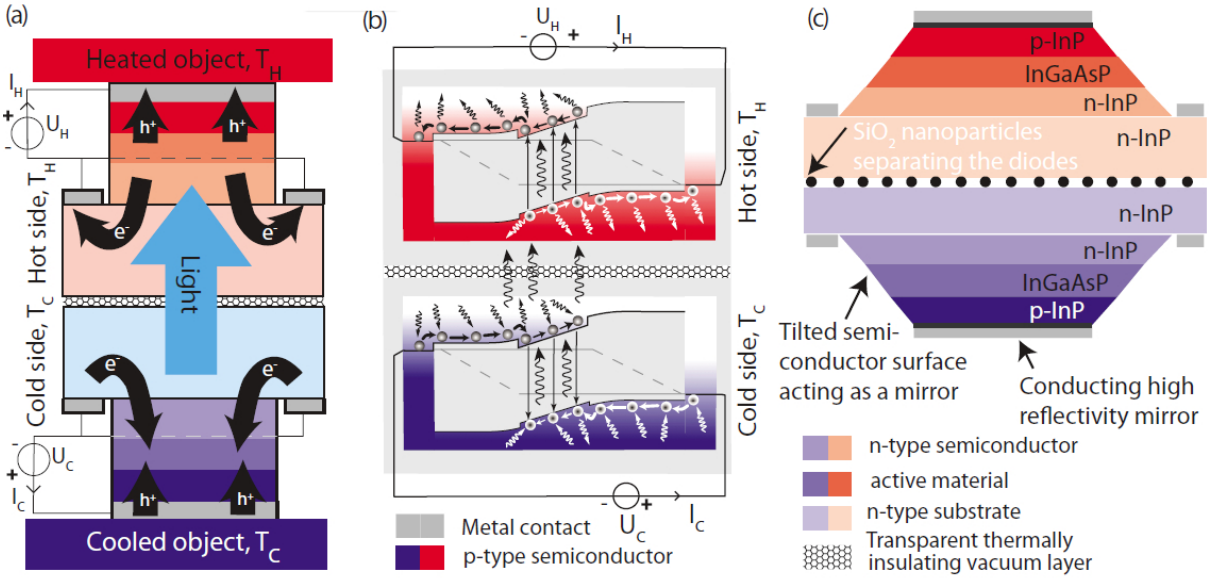

Figure 6: The thermophotonic heat pump is made of two optically coupled light-emitting diodes separated by a thin thermal insulation layer that is optically transparent. (a) Schematic picture of the flow of charge carriers and light in the THP structure. The LED on the cooled side emits light which partly gets its energy from the lattice heat. The heated LED structure absorbs the light and transforms it to electrical energy. (b) Shows the injection and recombination of charge carriers and the conduction and valence bands in both LEDs. (c) A schematic picture of the possible THP prototype.

The emitter and absorber LEDs are enclosed in the same semiconductor structure with an effectively homogenous refractive index throughout the device. Thus, the conventional problem in LEDs of light back scattering from the semiconductor/air interface is removed. Photons are emitted and absorbed in the same semiconductor structure and don't need to escape.

In the THP relatively large band gap (band gap $>> kT$) materials are used. Without energy recycling this would result in a poor coefficient of performance (COP) for the heat transfer because the energy required to emit a photon is much larger than the thermal energy kT. This problem is solved by the absorber diode which recycles the electrical energy back to the emitter diode.

A thin vacuum layer is introduced between the heated and cooled sides of the structure which thermally isolates them (Figure 6(a,c)). At the same time, the photon modes are nearly undisturbed, assuming the thickness of the vacuum layer is small compared to the wavelength of the photons. The unwanted conduction of heat from the heated side to the cooled side is effectively eliminated. This potentially allows cooling down to temperatures of approx. 50 K which is not possible with TE technology.

The diodes used in the THP structure will have a relatively large area and the active layer will be relatively thick. The obtained large volume active region will be able to produce reasonable cooling power while the energy of the injected carriers is still well below the energy of the emitted photons in the structure. This increases the amount of heat that each photon can carry (Figure 6(b)).

3 Key device properties

3.1 Contacts

The majority of semiconductor devices are driven by injecting electrical power into them. To be able to inject current into the semiconductor material, a high quality electrical contact between the wire and the semiconductor must be formed. For the THP, the most important properties for the contacts are that the contacts are ohmic and that their reflectivity is large. These properties are discussed in more detail below.

3.1.1 Ohmic contact

An ohmic contact on a semiconductor means that the voltage and current over the contact depend linearly on one another, as in ohms law. Ideally an ohmic contact is formed between a metal and an n-type semiconductor when the work function for the metal is smaller than the work function for the semiconductor i.e. $\Phi_m < \Phi_s$ as shown in Figure 7. In equilibrium the Fermi level E_F is constant across the junction and the potential barrier between the metal and the semiconductor is determined by the difference $\Phi_m - \chi_s$ between the metal work function and the semiconductor electron affinity χ_s. For a p-type semiconductor and a metal, an ohmic contact is formed when the work function for the metal is larger than the work function for the semiconductor i.e. $\Phi_m > \Phi_s$ (see Figure 8) [4].

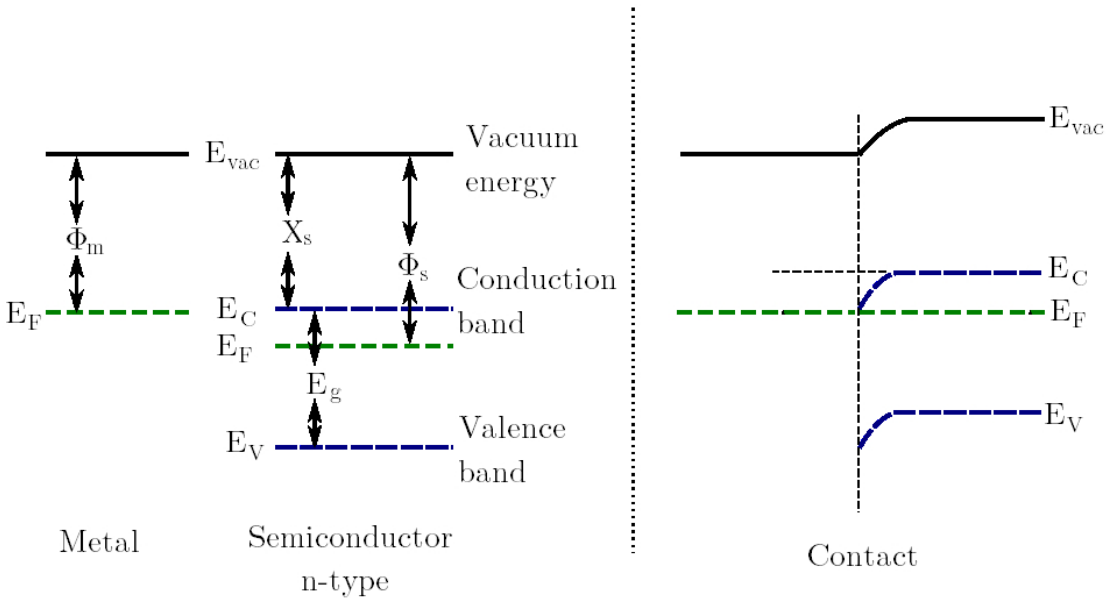

Figure 7: The energy band diagrams for a metal and an n-type semiconductor on the right and an ohmic contact formed by them to the left. In an ohmic contact the bands are bent so that the majority carriers do not see a potential barrier.

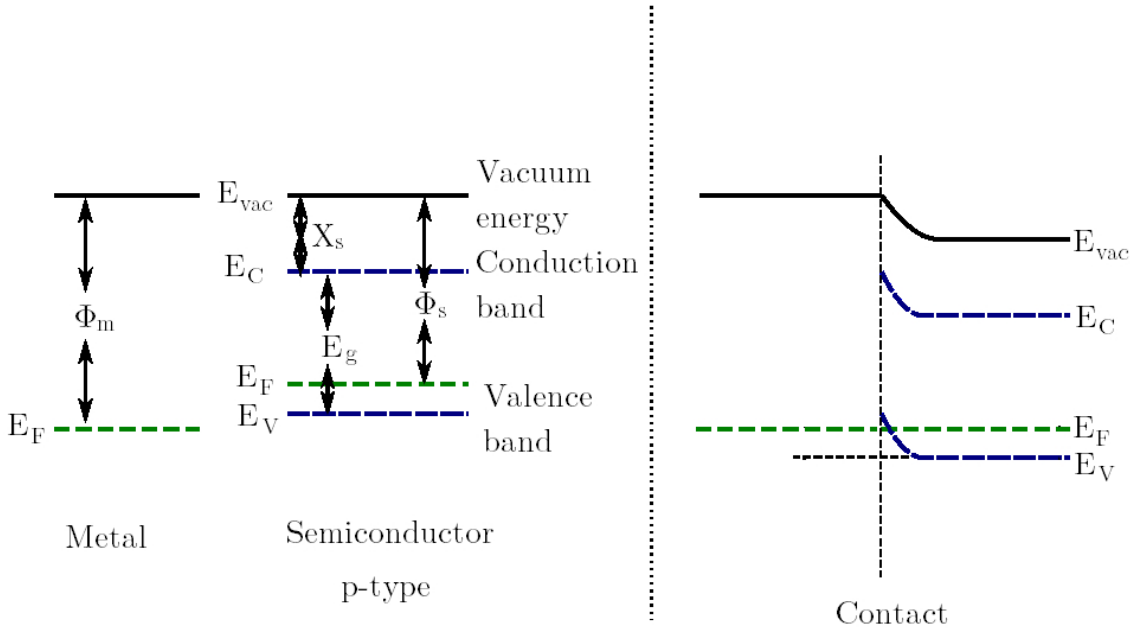

Figure 8: The energy band diagrams for a metal and a p-type semiconductor on the right and an ohmic contact formed by them to the left.

Another type of ohmic contact is created when the surface of the semiconductor is strongly doped and tunneling of the carriers over a potential barrier becomes possible [4].

When a metal and an n-type semiconductor whose work function is larger than the metals work function are in contact the electrons start to flow from the metal to the semiconductor until thermal equilibrium is reached. In thermal equilibrium the Fermi levels E_F are aligned and the metal and semiconductor have accumulated positive and negative charge, respectively, adjacent to the contact interface. The accumulated interface charge is accompanied by a band bending $\Delta V = \Phi_m - \Phi_s$ near the semiconductor surface. [4]

Low resistance contacts are needed in most devices where rectification is not sought for. Because of the low resistance, the efficiency of the device is not notably impaired due to the contact. In this work all the metallic contacts fabricated on semiconductor surfaces are intended as ohmic contacts.

3.1.2 Contact reflectivity

An important parameter in the performance of the THP is the reflectivity of the electrical metal contact which also acts as a mirror for emitted light in the structure.

When a plane wave encounters a boundary between two homogeneous media of different optical properties, it is split into two waves. The transmitted part of the wave proceeds into the second medium and the reflected part propagates back to the

first medium [11]. The fractions of power reflected and transmitted are represented by reflectivity (R) and transmissivity (T) of the interface, respectively. For a plane wave arriving to the interface perpendicular to it R and T are given by [11]

$$R = \left(\frac{\eta_2 - \eta_1}{\eta_2 + \eta_1}\right)^2 \tag{15}$$

$$T = 1 - R, \tag{16}$$

where η_1 and η_2 are the refractive indices for the incidence and refractive mediums. When the plane wave arrives to the interface at angle θ_1 with respect to the normal of the interface the reflectivity becomes polarization dependent. The mode of polarization is determined by the direction of the electric field vector. In case the electric field of light is perpendicular to the plane defined by the normal of the interface and the direction of propagation of the wave (Figure 1a) the reflectivity is given by [12]

$$R_\perp(\theta) = \left(\frac{\eta_1 \, cos\,\theta_1 - \eta_2 \, cos\,\theta_2}{\eta_1 \, cos\,\theta_1 + \eta_2 \, cos\,\theta_2}\right)^2, \tag{17}$$

where θ_2 is the refraction angle and dielectric materials were assumed. For polarization with the electric field in the plane of the normal of the interface and the direction of propagation (Figure 1b) the reflectivity is given by

$$R_\parallel(\theta) = \left(\frac{\eta_1 \, cos\,\theta_2 - \eta_2 \, cos\,\theta_1}{\eta_1 \, cos\,\theta_2 + \eta_2 \, cos\,\theta_1}\right)^2. \tag{18}$$

According to Snell's law the incidence and refraction angles are further related by

$$\theta_2 = arcsin\left(\frac{\eta_1 \, sin\,\theta_1}{\eta_2}\right). \tag{19}$$

The complex relative permittivity as a function of the angular frequency (ω) of the incident light of many contact metals can be calculated from the Drude model [13]:

$$\epsilon(\omega) = \epsilon_1 + i\,\epsilon_2 = \epsilon_\infty - \frac{\omega_p^2}{\omega^2 + \omega_\tau^2} + i\frac{\omega_\tau \omega_p^2}{\omega(\omega^2 + \omega_\tau^2)}, \tag{20}$$

where ϵ_1 and ϵ_2 are the real and imaginary parts of the permittivity, ω_p and ω_τ are the plasma and damping frequencies (constants) for a specific metal and ϵ_∞ is unity. The complex refractive index

$$\eta = n + i\,k \tag{21}$$

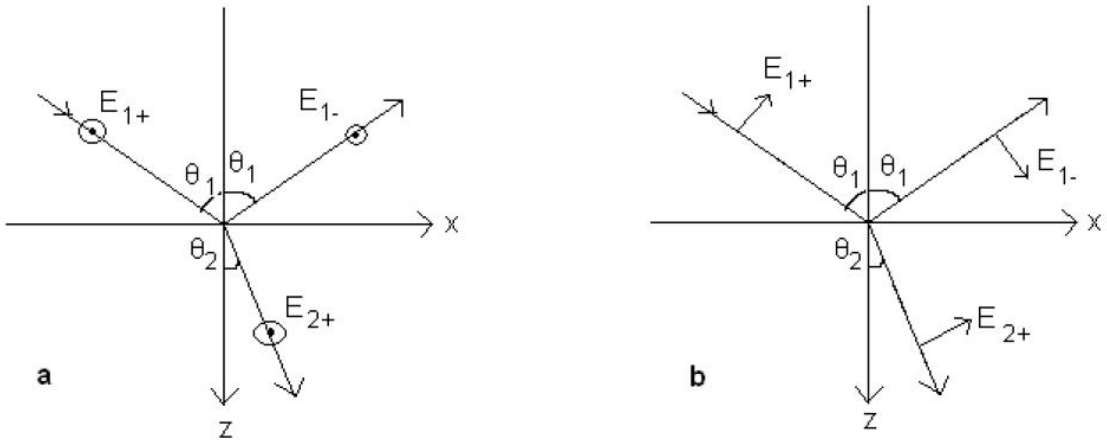

Figure 9: Polarization of the electric field of light. (a) The direction of the electric field is perpendicular to the plane of incidence (xz-plane) i.e. it only has a y-component. (b) The direction of the electric field is in the plane of incidence i.e. it lies in the xz-plane.

is related to the complex permittivity by $\epsilon = \eta^2$ so that

$$n = \sqrt{\frac{\sqrt{\epsilon_1^2 + \epsilon_2^2} + \epsilon_1}{2}} \tag{22}$$

$$k = \sqrt{\frac{\sqrt{\epsilon_1^2 + \epsilon_2^2} - \epsilon_1}{2}}. \tag{23}$$

The reflectivity for a specific metal in equations (17) and (18) can be calculated when the permittivity is known. The complex relative permittivities and reflectivities in air and InP for light arriving perpendicular to the interface for selected metals are shown in Table 1 using ω_p and ω_τ values retrieved from literature [14]. Light with a wavelength of 1670 nm was used in the calculations and the values of ω_p and ω_τ are expressed in electron volts.

Based on Table 1, the highest reflectivity would be obtained by using silver contacts. However, the electrical and mechanical properties of Ag-InP junctions are currently largely unknown, and their determination is out of scope for this work. Consequently, conventional three layer contacts of Au/Ni/Au or Au/Ti/Au are used.

3.2 Materials

The semiconductor materials used in this work are indium phosphide (InP) and indium gallium arsenide phosphide (InGaAsP). InP is a binary semiconductor and has a face-centered cubic ("zincblende") crystal structure. It has a direct band gap

Table 1: The complex relative permittivities, refractive indices and reflectivities in InP and air were calculated using the Drude model for ten metals commonly used as electrical contacts. The wavelength of light used in the calculations was 1670 nm. The reflectivities are calculated for the metal InP interface (R_{InP}) and the metal air interface (R_{air}). The top of the table uses Ref. [14] as the source for Drude parameters, while the bottom uses Ref. [13].

metal	$\omega_p\,(eV)$	$\omega_\tau\,(eV)$	ϵ_1	ϵ_2	n	k	R_{InP}	R_{air}
Ag	9.04	0.02125	-147.14	4.24024	0.1747	12.13	0.986	0.995
Au	8.89	0.07088	-141.08	13.5655	0.5703	11.89	0.954	0.984
Cu	8.76	0.0955	-135.95	17.6171	0.7538	11.68	0.938	0.978
Li	6.45	0.13	-72.232	12.8232	0.7514	8.532	0.894	0.960
Na	5.93	0.38	-49.554	25.8756	1.781	7.261	0.711	0.882
Al	12.04	0.1287	-254.32	44.2612	1.382	16.01	0.938	0.979
Ga	14.05	1.54	-66.539	140.096	6.654	10.53	0.599	0.843
In	12.8	0.46	-213.7	133.083	4.361	15.26	0.813	0.933
Zn	10.1	0.31	-156.5	65.8047	2.575	12.78	0.837	0.941
Cd	8.9	0.35	-116.57	55.4293	2.500	11.08	0.799	0.926
Al	14.754	0.0818	-389.19	43.007	1.088	19.76	0.967	0.989
Co	3.9674	0.03657	-27.489	1.4035	0.133	5.245	0.956	0.981
Cu	7.3894	0.009075	-98.051	1.2108	0.0611	9.902	0.993	0.998
Au	9.0260	0.02665	-146.61	5.3001	0.2188	12.11	0.983	0.994
Fe	4.0914	0.01822	-29.352	0.7451	0.06876	5.418	0.978	0.991
Pb	7.3646	0.2020	-90.613	24.938	1.297	9.607	0.856	0.947
Mo	7.4638	0.05108	-99.596	6.9213	0.3465	9.986	0.961	0.986
Ni	4.8849	0.04364	-42.144	2.5362	0.1952	6.495	0.954	0.982
Pd	5.455	0.01537	-52.969	1.1176	0.07677	7.278	0.985	0.994
Pt	5.1453	0.06918	-46.618	4.4373	0.3245	6.835	0.931	0.973
Ag	9.0136	0.01797	-146.31	3.5672	0.1474	12.10	0.988	0.996
Ti	2.5168	0.04736	-10.44	0.73019	0.1128	3.2340	0.933	0.961
V	5.1577	0.06062	-46.943	3.9152	0.2854	6.858	0.939	0.977
W	6.4099	0.0603	-73.05	6.0227	0.3520	8.5544	0.949	0.981

of 1.344 eV at 300 K [15]. The direct band gap makes InP useful in optoelectronic devices like LEDs and lasers. InP has high electron mobility and while InP itself is a good optical emitter the main benefit of it is in its use as a substrate for the quaternary compound alloy InGaAsP.

InP and InGaAsP can be perfectly lattice matched, i.e. their crystal structure can have identical lattice constants and they can be epitaxially grown one on the other if the relative portions of In, Ga, As and P are set to certain values. The band gap as a function of lattice constant for various III-V semiconductors is plotted in Figure 10. An InP/InGaAsP LED or laser (with InGaAsP as the active material) emits radiation with the wavelength ranging from 1.3 to 1.6 μm depending on the

relative portions of In, Ga, As and P in InGaAsP and other structure properties. Lasers and LEDs based on this material combination are central in the market in the 1.3 to 1.6 μm range and are used mainly in telecommunication and solar cell applications. The technology of processing InP/InGaAsP structures is mature and high quality samples can be fabricated, but the cost of an InP wafer is higher than some other compound semiconductors and especially higher than the cost of silicon. [17]

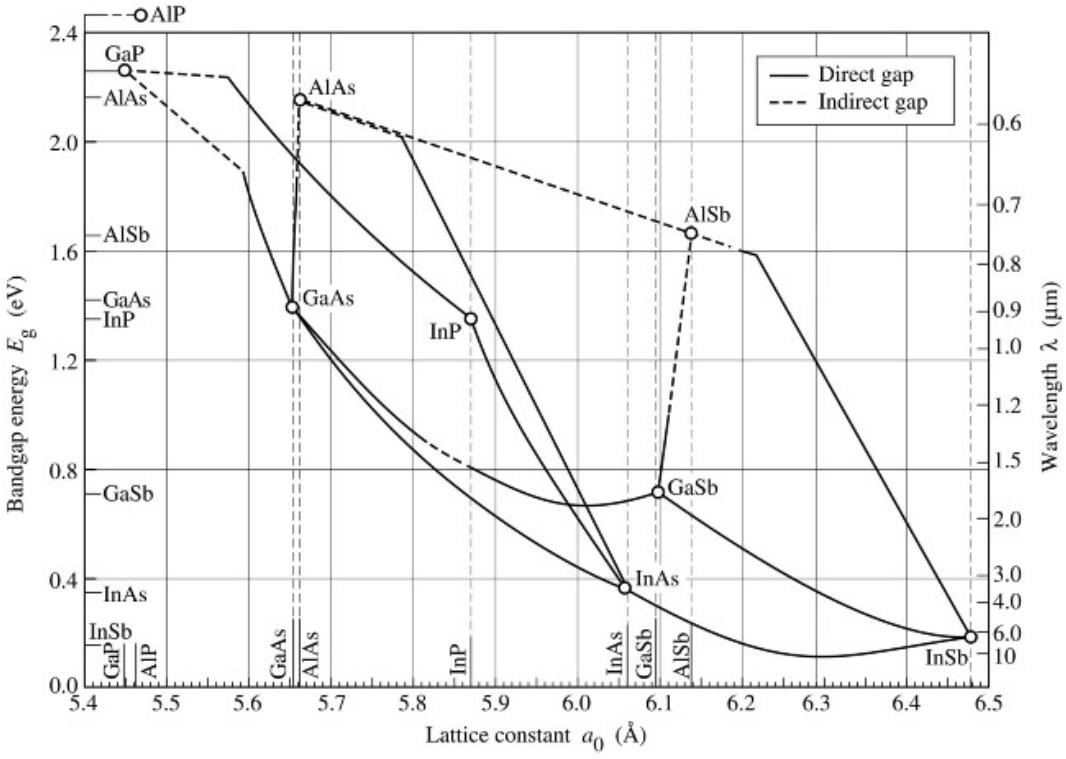

Figure 10: The band gap E_g as a function of the lattice constant a for different for various III-V semiconductors at room temperature. For InP $E_g = 1.344\,eV$ and $a = 5.8687\,A$. The gray vertical dashed line through InP represents the compositions where InGaAsP has a lattice constant equal to InP. [8]

A possible structure for the THP prototype using the above semiconductor materials is shown in Figure 11. In the structure, the two diodes are separated by a vacuum, in which nanoparticles have been grown. The gap is narrow enough to allow light, but not heat, to travel through it. The nanoparticles consist of a thermally and electrically insulating material like SiO_2 and they control the separation of the two diodes.

In this work, however, the focus is on fabricating and characterizing LED structures needed in a simplified laboratory prototype of the THP.

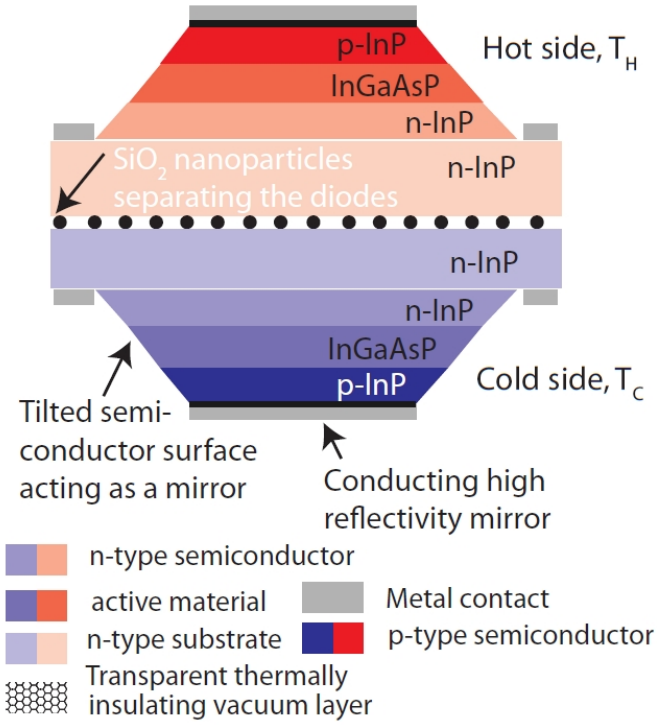

Figure 11: Schematic picture of the thermophotonic heat pump prototype.

4 Fabrication methods

4.1 Epitaxial growth

Epitaxial growth refers to a process of growing a single-crystal semiconductor layer on a single-crystal semiconductor substrate. The deposited film adopts the crystal lattice of the substrate. Epitaxial processes allow growing layered semiconductor samples that can be processed further to fabricate the desired final structure.

There are different methods to grow epitaxial material layers. In this work Metalorganic vapor phase epitaxy (MOVPE) is used. MOVPE is a specific kind of chemical vapor deposition (CVD) used to epitaxially grow materials. Benefits of MOVPE are the wide range of precursor source materials available, very flat and homogeneous surfaces and sharp material interfaces and precise control of the layer composition. [18].

In MOVPE the source chemicals, which are in gas form, are mixed with a carrier gas and injected into the reaction chamber. The substrate on which materials are to be deposited is attached to a heated susceptor. The metalorganic precursor source materials are decomposed in the hot zone above the substrate. When the precursors decompose, the actual materials intended to be grown (in this work III and V elements) are released and diffuse to the surface of the substrate. Atoms adsorb to the surface and can then diffuse on the surface, nucleate into the growing epilayer or desorb away from the substrate as illustrated in Figure 12.

All the samples in this work were fabricated using a MOVPE system manufactured by Thomas Swan Scientific Equipment Ltd. The III and V element source material precursors are metalorganic compounds: trimethylindium (TMIn) for indium, trimethylgallium (TMGa) for gallium, tertiarbutylarsine (TBAs) for arsenic and tertiarbutylphospine (TBP) for phosphorus. The source materials are held in temperature controlled baths in steel bubblers. Hydrogen (H_2) is used as the carrier gas. H_2 flows through the bubblers and is saturated with the vaporized source material. The amount of source material in the carrier gas is determined by the vapor pressure of the source compound determined by the temperature of the bubbler bath. The flow rate of the mixed gas is controlled by mass flow controllers. The source material gas flow from the bubblers is directed either to the mixing manifolds that lead the gas mixture to the reactor or to the vent line. The vent line is used to stabilize the flow of gas and to flush unwanted materials and residues from the reactor to the exhaust were toxic particles are oxidized and absorbed in a gas scrubber.

The MOVPE system is located in a semi clean room to ensure that unwanted particles don't enter the reactor in great amounts. The reactor is horizontal and made of quartz glass. Epitaxial growth takes place in atmospheric pressure. The substrate is placed on a 2×2 cm^2 graphite susceptor which is heated by a lamp outside of the reactor. The temperature is measured inside the susceptor and because of the gas flow through the reactor, in reality, the temperature at the sample surface is

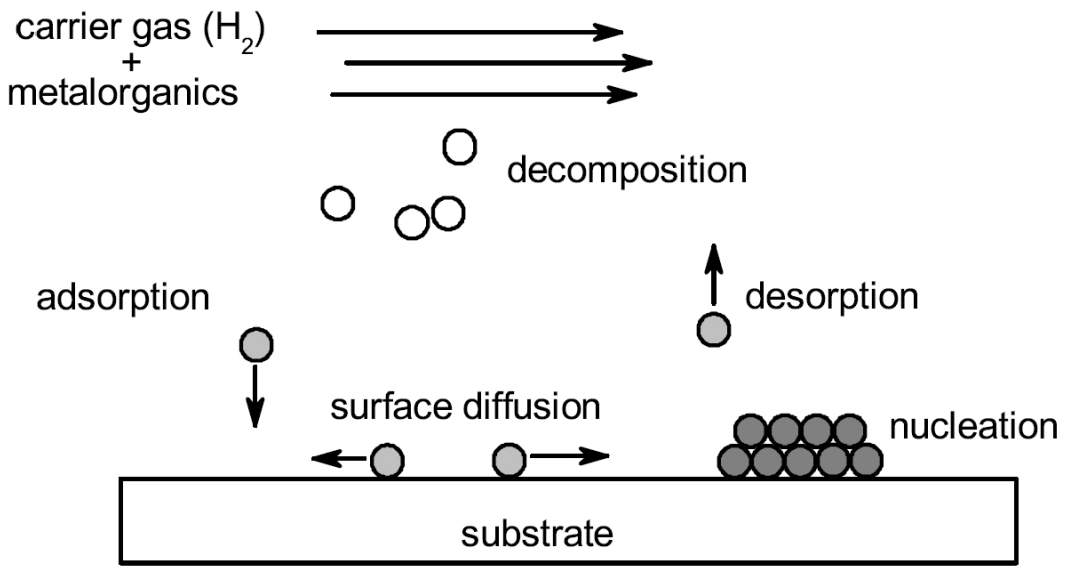

Figure 12: Schematic picture of the MOVPE epitaxial growth process. Carrier gas and metalorganic source material mixture is inserted into the chamber. The metalorganics decompose to III- and V-group elements. Atoms are adsorbed to the sample surface and can then diffuse on the surface, nucleate to the growing epitaxial layer or desorb away from the surface. [19]

somewhat lower than at the susceptor.

4.2 Lithography

Lithography is the process of transferring a geometric pattern to a layer of light-sensitive material called the photoresist as described in Figure 13. The photoresist consists of photosensitive polymers, solvent, sensitizers and other additives. The polymers either become soluble or polymerize when exposed to light. The solvent allows the resist to be spin coated. The sensitizers control the photochemical reactions and the additives can enhance processing and material properties. Positive photoresists are composed of phenol-formaldehyde novolak resins; the positive resist polymers are relatively insoluble in the photoresist developer, but after exposed to light, the polymers are easily dissolved in the developer. Negative photoresists contain polyisopreme polymers; after exposed to light, the polymers react and crosslink, or polymerize and become insoluble in the photoresist developer. [20]

Spin coating is a method of depositing thin films on substrates. An amount of liquid is placed on the substrate and the substrate is attached to a spinning axis. When the substrate is spun the liquid spreads out evenly on the substrate by centrifugal force. The longer the rotation is continued, the thinner the film will be. Photoresist is typically spun at 20 to 80 revolutions per second for 30 to 60 seconds. The

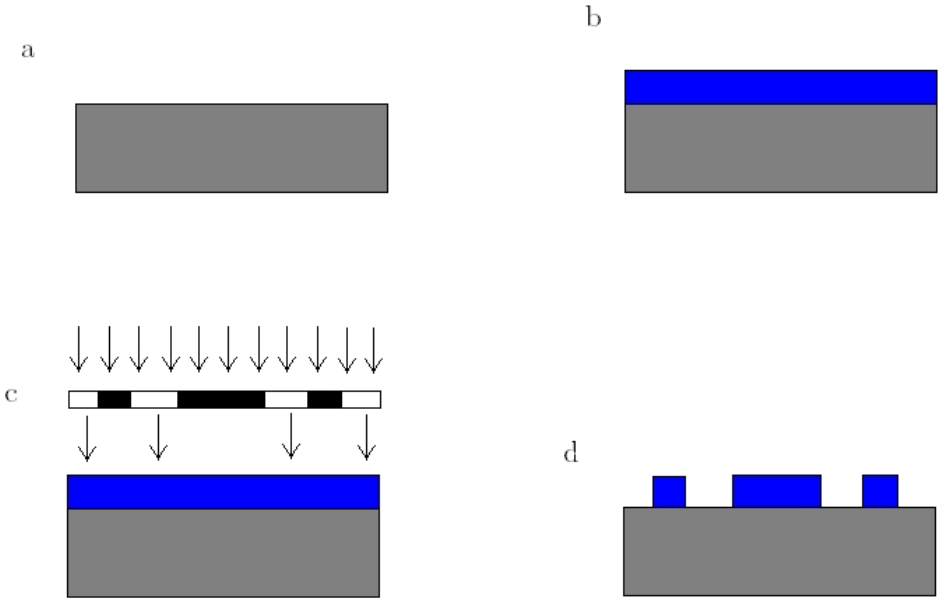

Figure 13: The steps in lithography. a) Clean substrate. b) A substrate coated with photo resist. c) Resist is exposed to light through the mask. d) Pattern on the resist layer after development.

thickness of the resist layer produced is typically 0.5 to 2.5 μm. [21]

The resist layer is exposed to light (often UV light) coming through a photomask. The mask lets light shine through certain parts, so that the areas which will be patterned are exposed. The resist will either get softer (positive resist) or harder (negative resist) when exposed. A reactive substance is used to remove the softer parts of the resist and leave the harder parts intact. This step is called development and a pattern is thus created in the resist layer on top of the wafer and this pattern can be used to introduce subsequent patterns to the actual wafer material. [22]

A photomask is usually made of a blank glass plate with an absorbing chrome film deposited on top. The chrome defines the lithography pattern because it is opaque. The masks aren't in contact with the substrate; there is some space and optics in between and the pattern from the mask is projected to the substrate. This allows the pattern on the mask to usually be four or five times larger than the projected pattern on the substrate.

In the development step the soft parts of the photoresist are removed by a reactive chemical called developer. The developer is poured on the substrate and spun in a similar process to resist spin coating. Traditionally, NaOH was a key ingredient in the developer but nowadays sodium is found to be a harmful contaminant in many semiconductor (especially MOSFET) fabrication processes. Now tetramethylammonium hydroxide (TMAH) is often used because it doesn't contain metal

ions.

Lithography typically precedes the process of etching, in which the resist pattern is transferred to the substrate. After this process the remaining hard photoresist is removed with liquid resist stripper. The stripper alters the resist chemically so that it dissolves from the substrate surface.

4.3 Etching

Etching is a microfabrication technique in which material is being removed from a wafer. The parts to be etched are defined by the pattern on the photoresist created by lithography. Thus etching transfers the resist pattern to the underlying material layers forming the device. Etching methods can be divided roughly into wet etching, in which the wafer is dipped into a liquid substance for example a solvent or acid and material is chemically removed, and dry etching, which often means bombarding the wafer with particles removing material through collision or chemical reaction. [22]

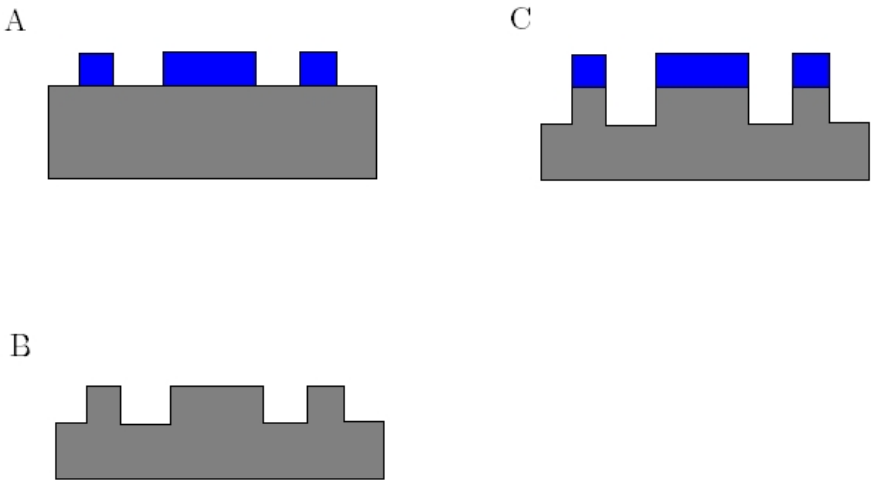

Figure 14: The basic steps in etching. A) Sample with photo resist pattern (etch mask) on top. B) An etching process removes material from the exposed parts of the sample. C) The etch mask is removed and the pattern on the sample remains.

When etching, often only a certain material or layer is supposed to be removed. The underlying layers and the etch mask must not be harmed. A specific etching system removes material of different compositions at different rates. The ratio of the etch rates in two materials is called selectivity. This ratio has to be taken into account when choosing the type and thickness of the etch mask. The harder and thicker the mask, the longer the wafer can be exposed to the etch process without damaging unwanted areas.

When wet etching, the etch rate is often isotropic, i.e. the lateral and horizontal etch rates are identical. This results in undercutting of the layer underneath the etch

mask, and the resolution of the pattern transfer suffers. Some wet etchants dissolve material in different crystal planes at different rates (anisotropic wet etching) but the etch process is then dependent on the orientation of the substrate.

Dry (plasma) etching allows true directionality in the etch process because of the control of the sputtering direction. Patterns of much smaller geometries and higher resolution can be produced with dry etching. Isotropic and anisotropic etching are illustrated in Figure 15.

Figure 15: Typical etching patterns of isotropic (1) and anisotropic (2) etching.

4.3.1 Reactive Ion Etching

Reactive Ion Etching (RIE) is a dry etching method where physical sputtering is combined with the chemical activity of reactive species. Sputtering is a process in which a solid target is bombarded with energetic particles and subsequently material is removed from the solid. The etch rate of RIE is higher than the combined etch rate of chemical reaction and sputtering and the etch profile is highly anisotropic [23]. Basic RIE equipment consists of a chamber that is pumped to high vacuum. The bottom surface of the sample to be etched is attached to a sample electrode.

In the RIE process an electric glow discharge is used to dissociate and ionize the feed gas (which is usually fluorine or chlorine based). The result is a plasma consisting of neutral atoms and molecules, electrons, radicals and positive and negative ions. The sample electrode is driven by a radio frequency (RF) power source. Since electrons have greater mobility than ions, the sample electrode ends up negatively charged i.e. a DC-bias voltage is created.

Neutral elements are transported from the plasma to the sample surface by diffusion. Positive ions are drawn to the substrate due to the electric field generated by the DC-bias. Reactive radicals adsorb on the sample surface and react with the atoms on it. The reaction process is enhanced by ion bombardment (sputtering) because it removes passivation layers from the sample surface formed by certain reaction products. The reaction product should have high vapor pressure so it desorbs away from the sample surface to the plasma and is then pumped out to the exhaust. [24]

4.3.2 Inductively Coupled Plasma-Reactive Ion Etching

Inductively Coupled Plasma-Reactive Ion Etching (ICP-RIE) means that there are two power sources operating the RIE etch process. The ICP-power creates a mag-

netic field which puts the particles of the gas in circular orbit. This allows confining the ions and electrons and thereby a plasma with high densities of radicals and ions is created. The capacitively coupled plasma (CCP) source directs the radicals and ions to the sample of the surface. By controlling the power of the CCP-source, the energies at which the particles hit the sample surface can be manipulated. With two power sources the etch process is more controllable and because of the high density plasma the etching process is faster than in other dry etching techniques. [25]

4.4 Evaporation

Evaporation is a method of thin film deposition of metals on a substrate. Evaporation of the source material (the metal to be deposited) takes place in a vacuum. This way the amount of other gas molecules is minimized in the process chamber. The evaporation of the source material requires energy that is commonly provided by heating the source with an electron beam which can have an energy up to 15 keV and the process is then called electron beam evaporation (EBE).

The source metal particles arrive at the substrate from a single direction and consequently the horizontal surfaces will get a thicker metal layer than the vertical walls. The deposit rate commonly varies between 0.1 and 2 nm/s. Evaporation is used for example in depositing the electrical (metal) contacts on to a LED. [26]

The evaporator used in this work is an Edwards E-beam Electron gun manufactured in 1989 (Figure 16). The system has 2 electron beam sources and 2 resistive sources in the same vacuum chamber. The minimum pressure 2×10^{-7} mbar. Minimum wafer size is 1 mm and maximum is 50 mm circular and four wafers can be inserted into the chamber simultaneously. Forbidden evaporation materials are Zn, AuZn and toxic materials. All semiconductor substrates are allowed.

In this work contacts consisting of typically Au/Ni/Au (thicknesses 5/10/70 nm) layers are evaporated on the substrate n-side and Au/Ti/Au layers (thicknesses 5/10/70 nm) on the p-side as electrical contact pads. Au is evaporated thermally by a strong current which vaporizes the gold. Ni and Ti are evaporated with the electron beam. Details of the evaporation process are presented in Appendix A.

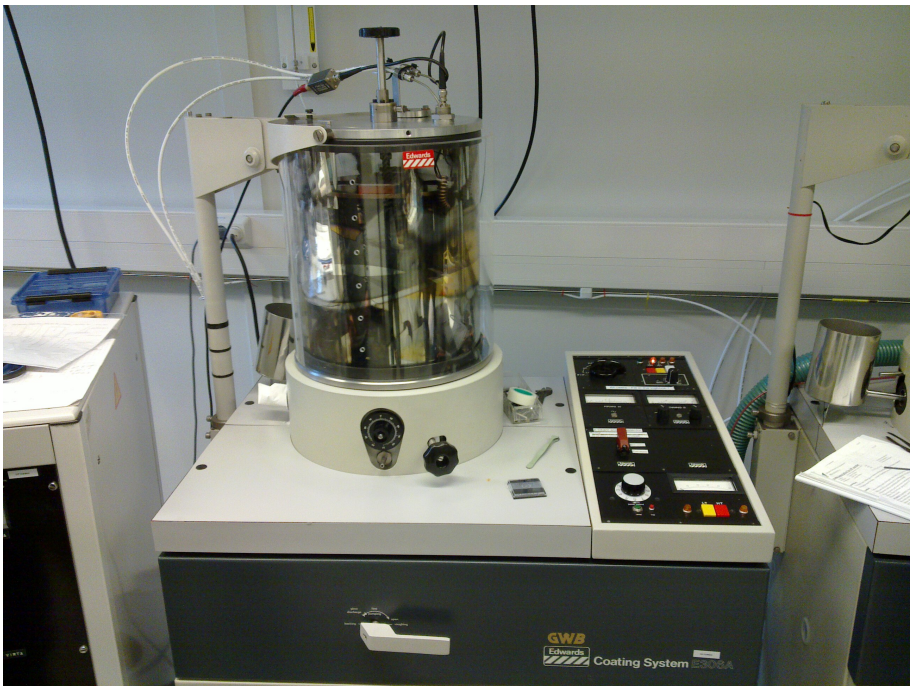

Figure 16: Edwards E-beam Electron gun manufactured in 1989. Installed in Micronova in 2002.

5 Characterization

This chapter briefly reviews the characterization methods that should/could be done for all diode samples to verify their properties.

5.1 X-ray diffraction

X-ray diffraction (XRD) is an experimental measurement method for the crystal structure, composition and layer thicknesses of crystalline materials. It is a popular method for studying semiconductors because it doesn't damage the sample. The basic idea of the measurement is to emit an x-ray beam against the sample surface and to measure the angle of incidence, the angle of departure and the intensity of the diffracted light.

For crystalline solids, x-rays are scattered from crystal planes. Bragg's law states that

$$n\,\lambda = 2\,d\sin(\theta_{hkl}), \tag{24}$$

where n is an integer, λ is the wavelength, d is the spacing between the planes in the atomic lattice and θ_{hkl} is the angle between the incident ray and the scattering planes [27].

The measurement setup consists of an x-ray source, mirrors, a monochromator, a sample holder, an analyzer and a detector. The x-ray source produces the x-ray beam that is directed by a mirror to the monochromator, which removes excessive wavelengths from the beam. The beam is directed from the monochromator to the sample, from which the diffracted radiation is measured by the analyzer-detector combination.

After the diffraction is measured from different angles, a computer plots the results and simulates a diffraction curve for the supposed structure that can be compared with the measured results. [27]

5.2 Atomic Force Microscopy

In Atomic Force Microscopy (AFM) the surface of a sample is studied using a very sharp needle that is connected to an oscillator. The tip of the needle might only be a few nanometers thick. With AFM it is possible to observe a fraction of a nanometers change in the vertical dimension and the horizontal resolution is about a nanometer depending on the size of the needle. The profile obtained from an AFM measurement is determined by the tip convolution, which means, that each of the pictures data points represents a spatial convolution of the shape of the tip and the shape of the studied form. As long as the tip is much sharper than the studied target, the profile is real, but if the target is sharper than the tip, the shape of the tip determines the image. The situation is illustrated in Figure 17.

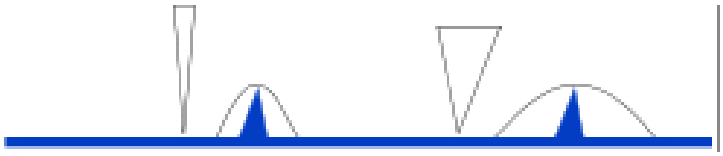

Figure 17: The effect of the size of the scanning tip in AFM on the resulting image. If the shape on the sample is sharper than the tip, the image will be determined by the size of the tip.

The van der Waals force is acting on the scanning tip and the size and direction of the force is determined by the distance between the tip and the sample. When the needle is sweeping the surface horizontally, the van der Waals force causes the scanning tip to oscillate. The amplitude of the oscillation is determined by the topography of the sample surface. [28]

5.3 Spectral photoluminescence

Photoluminescence (PL) is a process in which a material first absorbs a photon which excites an electron from the conductance band to the valence band and then emits a photon when the electron relaxes back to the valence band. If E_C is the energy of the conductance band and E_V is the energy of the valence band, the wavelength λ of the emitted photon can be approximated by

$$\frac{hc}{\lambda} = E_V - E_C, \tag{25}$$

where h is Planck's constant and c is the speed of light. [30]

A standard PL-measurement setup consists of a laser that is used to excite the measured semiconductor, a lens which collects and focuses the light emitted from the sample and a monochromator which analyzes the spectrum of the emitted light. The laser should emit light of a different wavelength than the measured semiconductor sample; otherwise luminescent light from the measured semiconductor cannot be distinguished from the light of the laser that is reflected of the semiconductors surface.

The result of the PL-measurement is the spectrum of the emitted light (PL spectrum), that is, the intensity of light as a function of the wavelength of light. From the PL spectrum the band gap can be approximated. Information about the composition of ternary and quaternary layers (e.g. the fractional amount of Ga in InGaAsP) can also be obtained from the spectrum. Optically active material impurities and recombination mechanisms can also be revealed by the measurement results. PL-measurement is often used to characterize semiconductors because it is a non-intrusive method; no physical contact with the sample is required.

5.4 Time-resolved photoluminescence

In a PL-measurement, the sample is continuously illuminated and the emitted light is continuously measured. In time-resolved photoluminescence (TRPL) the sample is excited with a very short light pulse which results in a decaying intensity of the emitted light over time. Measuring the decay of the luminescence allows estimating the recombination lifetimes of the sample. This technique is useful in measuring the minority carrier lifetime of compound semiconductors.

Typically the measured output of the TRPL measurement is expected to decay according to [8]

$$\frac{\mathrm{d}n}{\mathrm{d}t} = -An - Bn^2 - Cn^3, \tag{26}$$

where n is the carrier density and A, B and C are the recombination coefficients of Schockley-Read-Hall, radiative and Auger recombination, respectively.

5.5 I-V curve

The relationship between the current through a device and the voltage over it is known as the current-voltage (I-V) curve of the device. This often reveals some basic properties of the device. The I-V curve is obtained by for example sweeping a voltage of a certain range over the device and measuring the current at each voltage point. Needed equipment is a voltage source, an ammeter and electrical contacts to the device.

A simple I-V curve is that of the resistor, which is linear according to Ohm's law. The I-V curve for the p-n junction diode is ideally determined by the Shockley equation (Equation (1)). According to the Shockley equation the current through a diode depends exponentially on the applied voltage.

The I-V curve of a diode tells much about its ability to perform optimally. For instance, if there is significant current going through the diode when the voltage is less than zero (reverse bias), then it might mean that there is an alternative current path through the p-n junction and the device doesn't work optimally.

5.6 Electroluminescent cooling measurement

The most straightforward measurement for observing the electroluminescent cooling of the THP would be by directly measuring the temperatures at the diodes on the cooling and heating sides. In addition to the direct measurement, the heat transfer between the two diodes can be measured indirectly. This is convenient, since the temperature differences between the diodes in the prototype structure will probably be very small and hard to detect.

In the indirect measurement setup a voltage (U_1) is applied to the emitting diode and the current (I_1) is measured so that the I-V curve of the emitting diode is obtained. The light that the diode on the cool side emits (with average photon energy of about $hf = E_{g,InGaAs}$) is partly absorbed by the diode on the heated side and gives rise to a current (I_2), which is measured by an ammeter. The measurement setup is presented in Figure 18.

The rate at which electrons flow into the diode on the cool side is I_1/q, where q is the electronic charge. The rate W at which the diode emits photons is less than or equal to the rate of injected electrons,

$$W \leq \frac{I_1}{q}. \tag{27}$$

The photons absorbed on the hot side give rise to a current I_2 satisfying

$$\frac{I_2}{q} < W. \tag{28}$$

The emitted power is therefore at least W and for the measured currents it holds

$$I_2 < I_1. \tag{29}$$

The electrical power consumed by the cool side due to the applied voltage is $P = U_1 I_1$. When the average photon energy hf is known the optical power received by the diode operating as the receiver is at least $I_2/q \times E_g$. This power is also at least equal to the emitted power generated by current I_1. If

$$\frac{I_2}{q} hf > P \tag{30}$$

holds, it means that the emitted photons transfer more energy than is injected as electrical power into the emitter diode. The difference originates from lattice heat of the emitter, and therefore the emitter cools down by the emission.

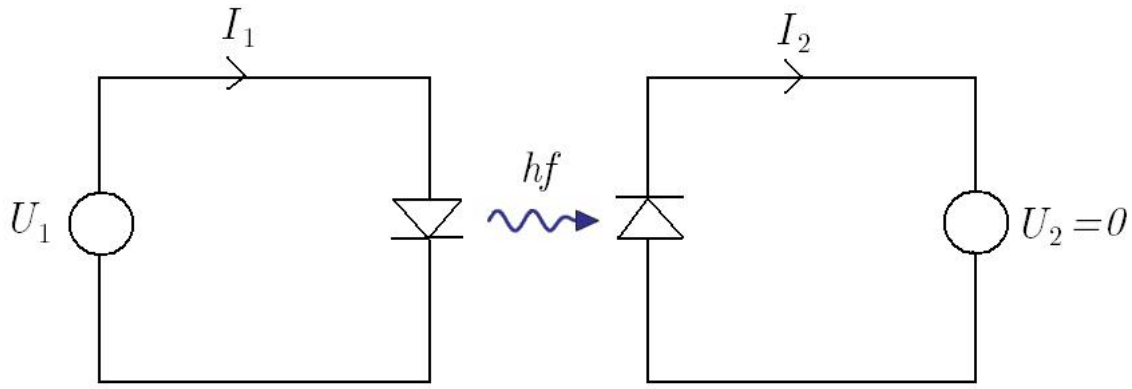

Figure 18: Schematic picture of the indirect measurement of the heat transfer in the thermophotonic heat pump prototype. The cool side of the circuit is on the right and the hot side of the circuit is on the left. By applying the voltage U_1 to the cool side and measuring the currents I_1 and I_2, cooling can be detected.

6 Results

6.1 Samples fabricated

In order for a THP prototype structure to act as a cooling device, high quality large area p-n junction diodes have to be fabricated. During this work, 63 semiconductor samples were grown with MOVPE of which 30 were grown on semi insulating (S-I) InP substrates and the rest on double polished n-doped InP substrates. The samples that were grown on an S-I substrate were either completely intrinsic or had a single doped layer in order to make Hall measurements to check the doping concentrations. The samples grown on an n-InP substrate were doped and of these 22 were fabricated with an InGaAs active layer and were intended as light-emitting or light-absorbing p-n double hetero junction diodes. On intrinsic samples, photoluminescence (PL), X-ray diffraction (XRD) and microscopic measurements were made. In case of the doped samples, the measurements were complemented by Hall and I-V measurements, as well as electroluminescence measurements in case of p-n junctions.

Samples grown on S-I and n-doped substrates were grown with several different layer thicknesses and material compositions. These samples were characterized with methods presented in Chapter 5. In this chapter, selected measurement results for samples whose layer thicknesses and compositions are listed in Table 2, are presented.

Table 2: A list of samples whose properties are discussed in this Chapter.

THP	Substrate	Structure (top to bottom)	Layer thickness (nm)
001	InP S-I	5 x i-InGaAs/i-InP MQW	
008	InP S-I	i-InP/i-InGaAs/i-InP	200/200/200
035	n-InP	p-InP/i-InP/i-InGaAs/n-InP	100/50/100/100
036	n-InP	p-InP/i-InP/i-InGaAs/n-InP	100/100/100/100
037	n-InP	p-InP/i-InP/i-InGaAs/n-InP	100/150/100/100
038	n-InP	p-InP/i-InP/i-InGaAs/n-InP	100/0/100/100
039	n-InP	p-InP/i-InP/i-InGaAs/i-InP/n-InP	100/50/20/50/100
040	InP S-I	i-InP/i-InGaAs/i-InP	150/20/150
041	n-InP	p-InP/i-InP/i-InGaAs/i-InP/n-InP	100/50/100/50/100
049	n-InP	p-InP/i-InP/n-InP	100/100/100
056	n-InP	p-InP/n-InP	300/300
057	n-InP	p-InP/i-InP/n-InP	100/300/100
059	InP S-I	i-InP/i-InGaAs/i-InP	400/300/300
060	n-InP	p-InP/i-InP/i-InGaAs/n-InP	100/150/100/100
061	n-InP	p-InP/i-InP/i-InGaAs/n-InP	500/150/100/100
062	n-InP	p-InP/i-InP/i-InGaAs/n-InP	500/150/100/100
063	n-InP	p-InP/i-InP/i-InGaAs/n-InP	100/150/100/100

6.2 XRD-measurements

X-ray diffraction (XRD) measurements were made to selected samples in order to determine whether the active layer (InGaAs) is lattice matched to InP. Information about the composition of the active layer (the relative amounts of In, Ga and As) can possibly also be obtained with XRD. The measurements were performed using a Philips X'Pert Pro x-ray diffractometer.

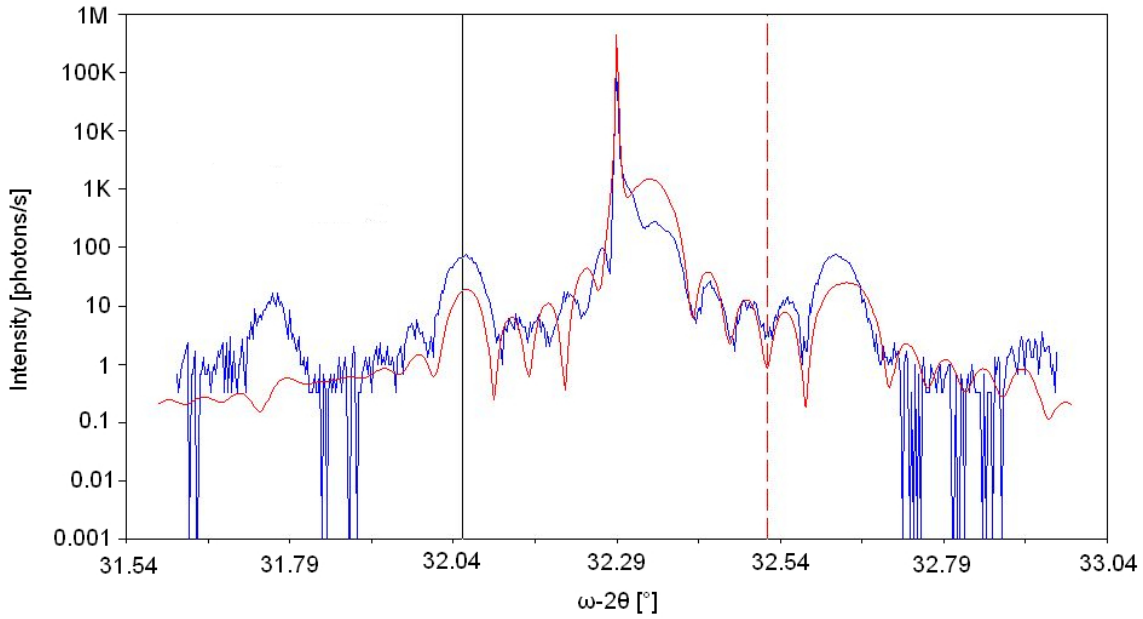

Figure 19: XRD-measurement results for sample THP001. The red line is the simulated (expected) result for a similar structure and the blue line is the actual measurement.

Results of the ω-2θ XRD-measurement made to sample THP001 are shown in Figure 19. The blue line is the actual measurement of the real sample THP001, which is a 5 x i-InGaAs/i-InP MQW structure. The red line is a computer simulation of a 5 x InGaAs/InP MQW structure with a thickness of $d_{\mathrm{QW}} = 8.3$ nm for the InGaAs layers and $d_{\mathrm{barrier}} = 7.6$ nm for the InP layers and with the amount of In in the InGaAs layer at 50.5 %.

The maximum at 32.29° is the diffraction from the InP substrate. On the left side of the maximum there are two and on the right side there are three smaller peaks, known as satellite peaks. The satellite peaks are caused by the average diffraction of the MQW and the distances between the peaks are a direct result of the thickness of the period T (the sum of the thicknesses of an InGaAs and an InP layer) [27]. Between the satellite peaks, there are three smaller peaks. The number of the smaller peaks is the number of QWs less two, that is $N_{\mathrm{peaks}} = N_{\mathrm{QW}} - 2$ [29]. The distance between two smaller peaks is proportional to the thickness of the period, i.e. $\Delta\theta \propto n\,T$, where n is some integer.

From Figure 19 it can be seen that the angular positions of the satellite peaks of the simulation coincide with measured ones. This confirms, that the $T = d_{\mathrm{QW}} + d_{\mathrm{barrier}} = 8.3\,\mathrm{nm} + 7.6\,\mathrm{nm} = 15.9\,\mathrm{nm}$, as simulated. However, some other combination of d_{QW} and d_{barrier} whose sum is 15.9 nm could also be possible.

The results from the XRD-measurement are that the barrier thickness is 15.9 nm and that there are five quantum wells. The simulated curve depends on the materials, their thicknesses, compositions and tensions. Many simulations were tried with different properties but the one that is plotted, fitted best to the measured curve. However, the solutions to the simulation curve aren't unambiguous, i.e. many combinations of parameters might produce very similar diffractions curves. In order to obtain the material composition of the layers, complementary measurements would have to be made.

6.3 Atomic Force Microscope measurements

Atomic force microscope measurements were used to characterize the surface of the semiconductor samples. The AFM-system used is model NTegra fabricated by NT-MDT. Selected 3D AFM images are shown in Figures 20-23.

Figure 20 shows a 3D view of the sample surface of THP056 which is very smooth. The picture shows atomic steps formed during the growth as well as periodic grooves that are about 4 μm wide and 1.6 nm deep. Figure 21 shows another similar picture of THP060.

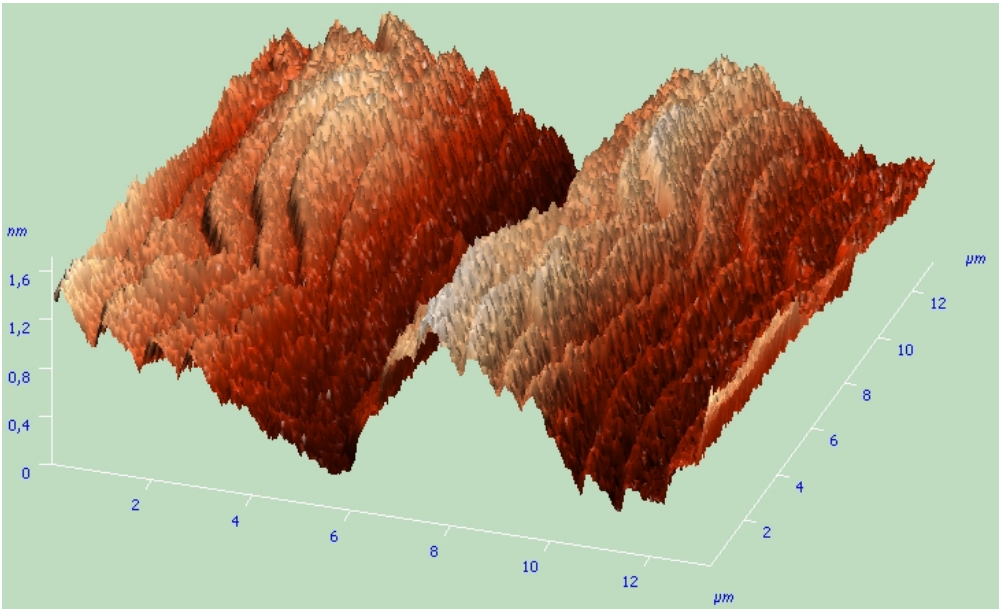

Figure 20: AFM image of the grown surface of sample THP056. The sample surface is very smooth and atomic steps are clearly visible.

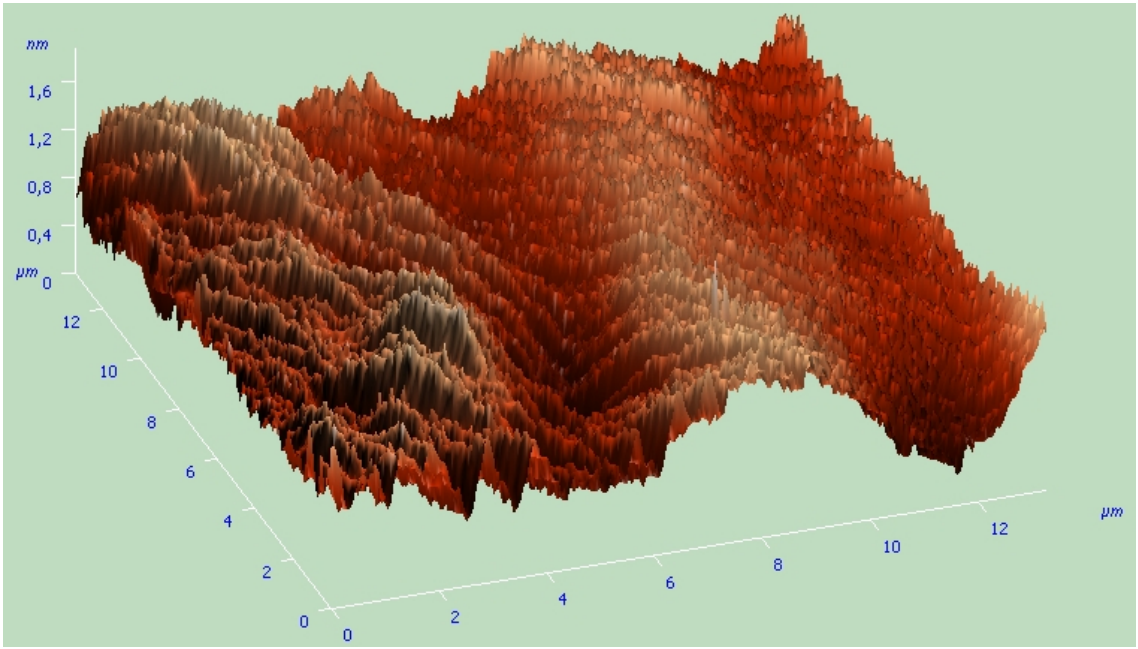

Figure 21: AFM image of the surface of sample THP060.

Figure 22 shows the picture of an intrinsic sample THP059. The grooves are slightly more pronounced, about 10 μm wide and 4 nm deep, but still with very good surface quality.

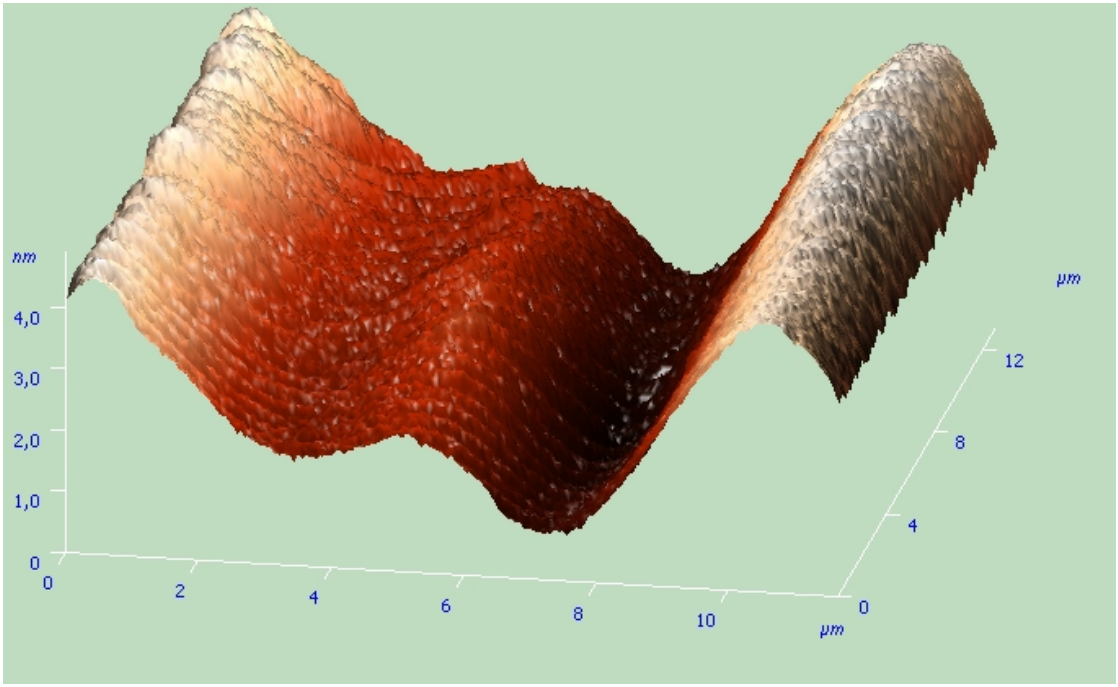

Figure 22: AFM image of the surface of sample THP059.

Figure 23 shows a 3D AFM image of sample THP060. On the sample surface there

is a peak that is over 2 μm high, and around the peak there is a pit that may reach all the way through the p-type layer. In general the surface quality is relatively high and locating these pits is challenging. However, these kinds of defects are one of the main candidates for the large leakage currents that will be discussed in Section 6.5.

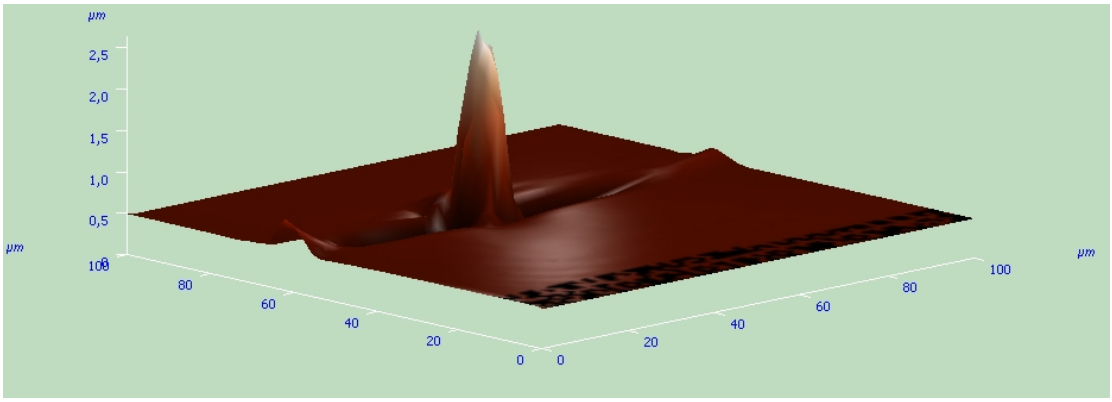

Figure 23: AFM image of the surface of sample THP060. The image shows that there is a large defect on the surface.

6.4 PL-measurements

The results for the PL-measurement for selected samples are shown in Figures 24-26. THP008 had originally a relatively high PL intensity and it is therefore used as a reference sample in the PL-measurements. THP008 was grown on a semi insulating InP substrate with an intrinsic InP layer, an InGaAs layer and another intrinsic InP layer whose thicknesses were all 200 nm.

Figure 24 shows that all doped samples THP035-038 (see Table 2 for the properties of these diodes) have significantly lower PL intensity than the intrinsic reference sample THP008. This is partly explained by the thinner active region in samples THP035-038, but also doping plays a role: the generated carriers are spread onto a relatively large area due to the p-n junction. The electric field in the active layer is also expected to reduce the radiative recombination rate of electrons and holes.

Figure 25 shows the effect of doping and active layer thickness on the PL intensity in more detail. Samples THP008 and THP040 are both intrinsic, with an active region thickness of 200 nm and 20 nm, respectively. The PL intensity for sample THP008, however, is only about 50 % larger than that of sample THP040. The wavelength of the maximum intensity is also blueshifted by about 100 nm mainly due to the quantization of the carrier energy levels in the 20 nm wide quantum well. The PL intensity of sample THP040 is 10 times larger than the PL intensity for sample THP039, which differs from sample THP040 only by the presence of doped material layers next to the active layer, indicating again that doping indeed reduces the PL intensity. In sample THP041 the thickness of the active region is increased 5-fold with respect to sample THP039, resulting in a PL intensity that is thrice the

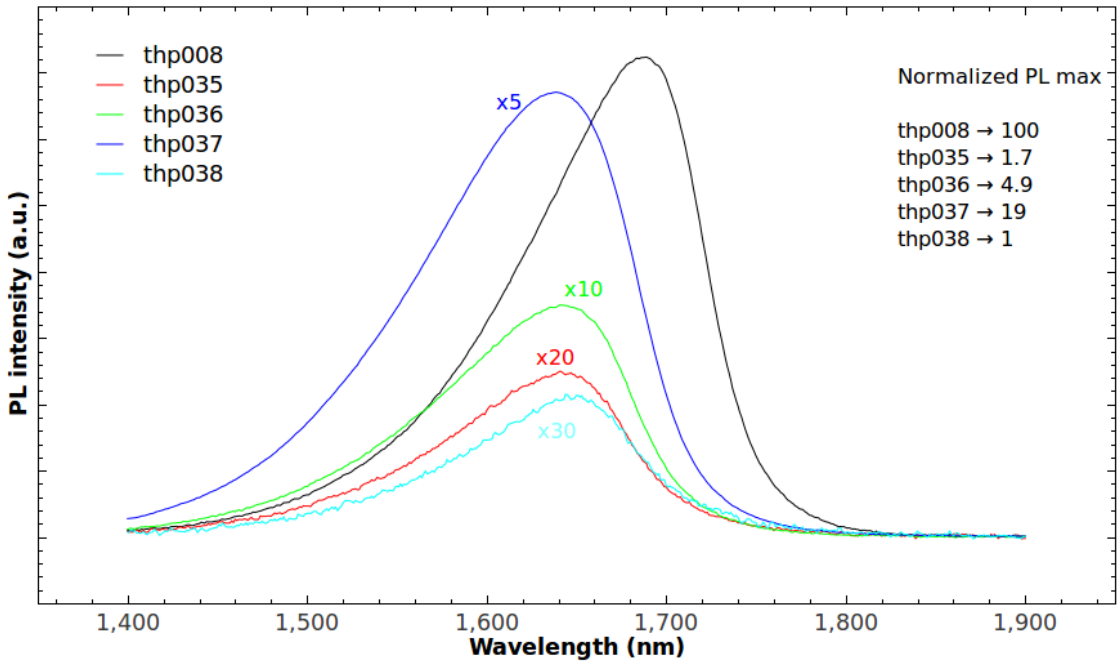

Figure 24: PL intensity as a function of wavelength for an intrinsic reference sample THP008 and samples THP035-038 where the active region distance from the p-type layer is varied. The markings x5, x10 etc. show the scaling of the intensity. Normalized PL max indicates the maximum intensity emitted by a specific sample with the maximum of THP008 normalized to 100. The maximum intensity increases as the distance of the active region from the p-type layer increases.

intensity of THP039. As the active region thickness increases, the relative increase of the PL intensity for doped samples therefore seems to be far greater than for the intrinsic samples. This is most likely due to the reduction of the electric field in the p-n junction due to the thicker intrinsic active region.

Figure 26 shows how the current spreading by a thick p-type layer, changes in the III-V ratio used in the growth process and the active layer thickness affects the PL intensity. THP008 and THP059 are intrinsic samples with 200 and 300 nm thick active regions, respectively. The 50 % increase in active layer thickness resulted in a PL peak that was only about 15 % higher. Rest of the samples THP060-063 were doped samples with 150 nm thick active layers and 100 nm (THP060, THP063) and 500 nm (THP061, THP062) thick p-type layers. THP063 was grown with a dirty reactor and THP062 was grown with a higher III-V ratio. The PL peak of THP063 is almost as high as that of THP060 indicating that the cleanliness of the reactor does not play a major role. Furthermore both peaks are only about 10 % lower than that of THP008. The PL intensity of samples THP061-062 with 500 nm p-type layers is clearly lower than the intensity of sample THP060 with the 100 nm p-type layer. This suggests that the more efficient current spreading by the thicker p-type layer decreases the radiative efficiency. The doped samples were grown using a zinc

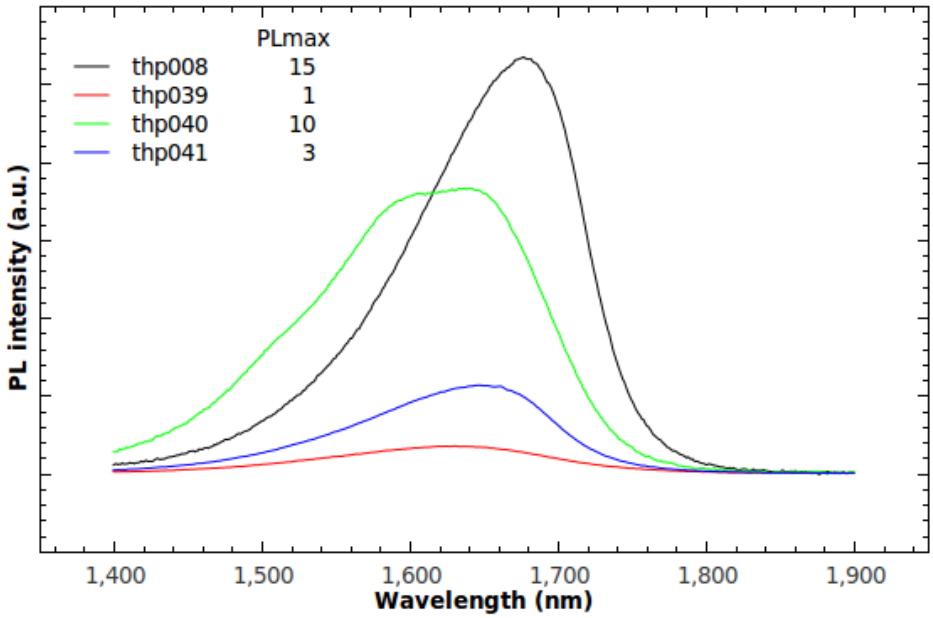

Figure 25: PL intensity as a function of wavelength for samples THP039-041. PL max is the relative maximum intensity emitted by a specific sample. The PL measurement shows that for an intrinsic sample THP040 with an active region of 20 nm (one tenth of the active region thickness of sample THP008) the maximum intensity is reduced only by about 30 %, while for the doped samples THP039 and THP041 a five fold increase in the thickness of the active region increases the PL intensity by a factor of three.

precursor flow of 2.0 sccm while the samples in Figure 24 and 25 were grown with a zinc precursor flow of 3.5 sccm. As the PL intensity of the samples grown with the larger zinc precursor flow of 3.5 sccm was clearly smaller than for the samples grown with 2 sccm there seems to be a link between high Zn concentration and a low PL peak in general.

Generally, the PL measurements are relative measurements, i.e. the absolute value for the coefficient of performance cannot be calculated out of the results shown in this section due to limitations in the measurement setup. The use of sample THP008 as a reference sample allows the samples in different measurements to be compared to one another.

6.5 I-V measurements

The I-V curves of the fabricated semiconductor samples were measured by applying a voltage sweep across the diode and measuring the corresponding currents. To make the measurements, electrical ohmic contacts were deposited on both the n-type and p-type materials. The samples were connected to the I-V probe station by

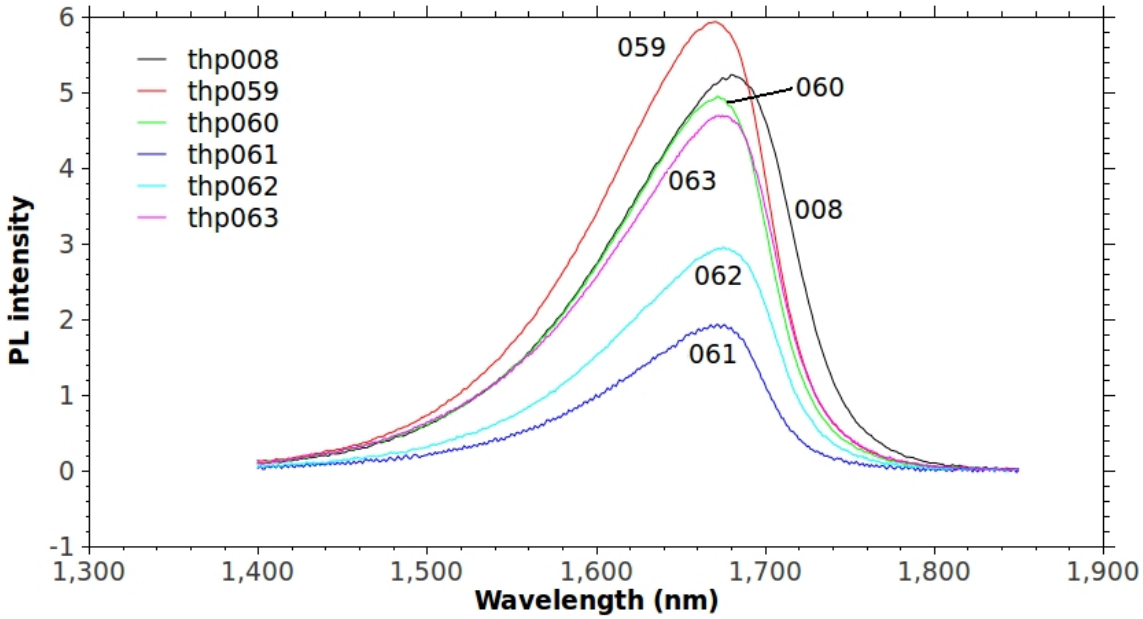

Figure 26: PL intensity as a function of wavelength for samples THP059-063. The measurement shows that when the flow of p-type dopant precursor was reduced from 3.5 sccm to 2.0 sccm, the PL peak for THP060 with a 150 nm active layer was almost high as that of the intrinsic reference sample THP008 with an active layer thickness of 200 nm. In Figure 25, THP041 with an active layer thickness of 100 nm and a zinc flow of 3.5 sccm had a PL peak one fifth of the peak of THP008.

pressing electrical probe needles against the fabricated contact pads. In some cases, conducting wires were soldered to the contact pads in order to allow smaller contact resistance and to prevent possible damage done by the sharp probe needles to the semiconductor epilayer underlying the metal contact.

I-V curves of the p-n junctions of four selected samples are shown in Figure 27. Samples THP035 and THP037 are double heterostructure diodes with an InGaAs active layer and THP049 and TH056 InP p-n homojunction diodes. This should make the threshold voltage for THP035 and THP037 about 0.7 V and for THP049 and THP056 about 1 V. The surface area of all samples was originally $\sim 1\,\mathrm{cm}^2$. THP035 was cut into a piece with an area of $\sim 1\,\mathrm{mm}^2$ before measurement while the rest were measured as originally fabricated. Samples THP035 and THP037 were contacted by evaporating isolated contact pads of $\sim 1\,\mathrm{mm}^2$ on both the n- and p-type sides. The p-side contacts are Au layers of thickness 50 nm. The n-sides have Au/Ni/Au multimetal contacts with thicknesses of 5/10/30 nm in order of deposition. THP049 and THP056 were contacted by evaporating the whole sample area on both the n- and p-sides. The p-sides have Ti/Au 10/100 nm multimetal contacts and the n-sides have Ni/Au 10/100 nm contacts. Additionally, in case of sample THP056, pieces of InZn were soldered on top of the p-side metal contact and pieces of In were soldered on the n-side metal contact in order to get very thick

blocks of relatively soft metal, into which the probe needles could be pushed for maximum conductivity.

Figure 27 also shows current through an ideal InP diode which is extremely small when $V < 0.9\,\mathrm{V}$. Of the fabricated samples, however, only THP056 shows features resembling the ideal diode. It does have a relatively large shunt resistance allowing fairly large currents under reverse bias ($V < 0$) but it also has a clear threshold near $V = 1\,\mathrm{V}$. THP037 conducts even more current under reverse bias. THP049 is an example of a badly damaged sample, which acts completely like a linear conductor. THP035 shows diode-like behavior, but the current rises fast under forward bias without a clear threshold which could also indicate high contact resistance. The diodes generally conduct too much current, which suggests that there are alternative current paths through the diode.

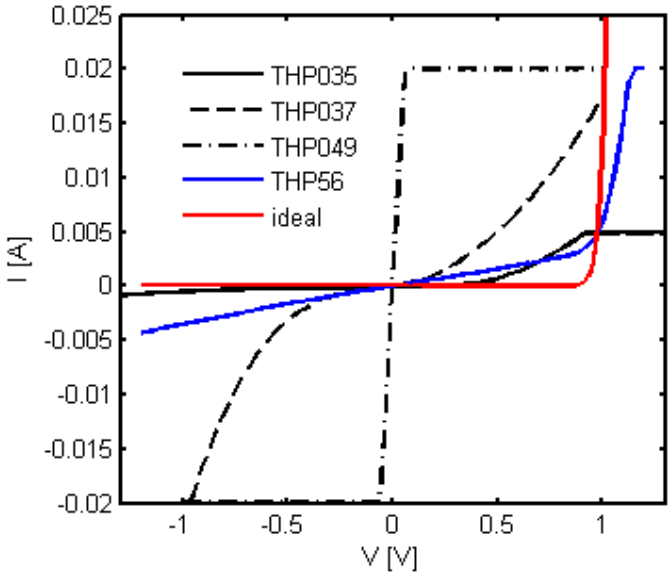

Figure 27: I-V curves of the p-n junctions of four selected diodes and the ideal diode I-V curve. Sample THP056 shows most diode-like properties, but has an unusually large shunt resistance.

The ideal I-V curve of Figure 27 is calculated with Equation (1). According to the Einstein relation [31] the diffusion constants of carriers can be written as

$$D_n = \frac{kT}{e}\mu_n \quad \text{and} \quad D_p = \frac{kT}{e}\mu_p \tag{31}$$

where $\mu_{n,p}$ are the electrical mobilities of electrons and holes and other required constants are

k	$1.380650410 \times 10^{23}$ J K^{-1}
T	298 K
A	1 cm^2
n_i	1×10^{12} m^{-3}
N_A	1×10^{24} m^{-3}
N_D	1×10^{24} m^{-3}
μ_n	0.01 m^2/(V s)
μ_p	0.1 m^2/(V s)
τ_n	1×10^{-8} s
τ_p	1×10^{-8} s.

I-V curves of the p-type and n-type layers were also measured to verify that the metallic contacts perform adequately. I-V curves for the n-contact to n-contact and p-contact to p-contact measurements for selected samples are shown in Figure 28 and 29, respectively.

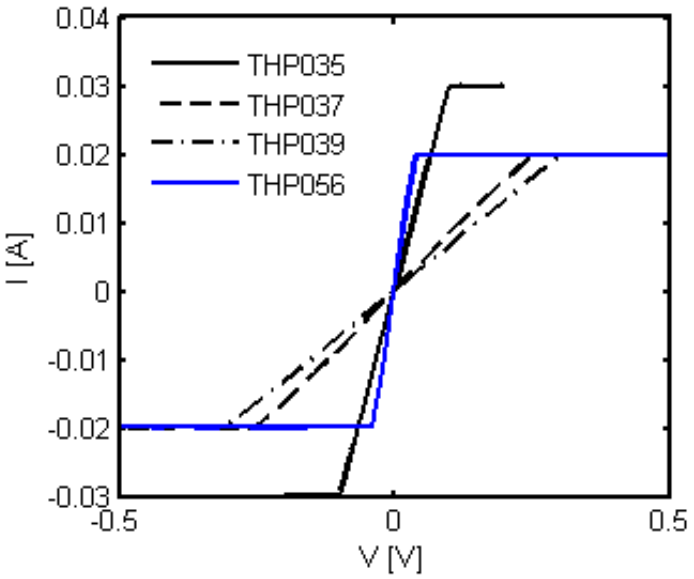

Figure 28: I-V curve of the n-type layer of four fabricated samples. The curves verify that the n-type contacts perform as expected.

The n-type layers in Figure 28 show a linear behavior with the resistance between 3 and 15 Ω. Linear behavior with relatively low resistance is expected and confirms that the metal contacts are ohmic and that the doping levels for the n-type layers are appropriate.

Figure 29 shows the I-V curves of the p-type layers of selected samples. Sample THP042 shows linear behavior, but its resistance is relatively high, about 4.2 kΩ, while THP037 has significantly lower resistance (about 150 Ω) but the I-V curve shows some rectifying properties. Sample THP056 shows diode like behavior, which might result from non-ohmic (rectifying) contacts. Interpreting the measurement results is, however, complicated by the p-type layers being located on top of a

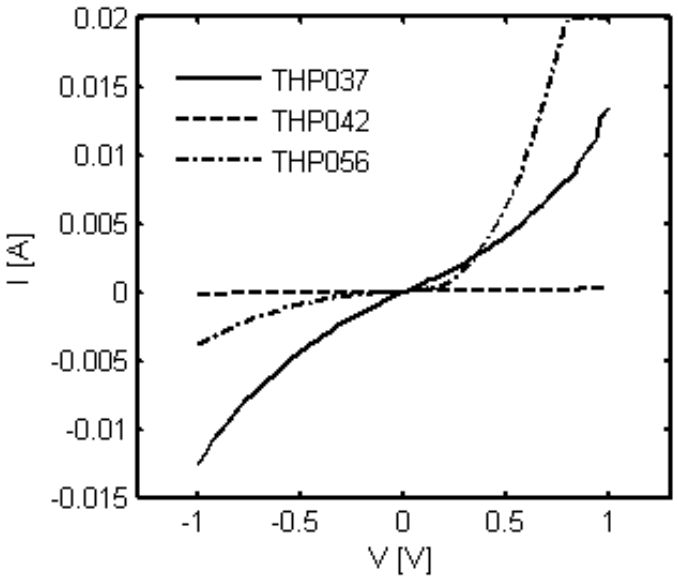

Figure 29: I-V curve of the p-type layer of three selected samples. The I-V curves are expected to have a large resistance due to very small layer thickness. The rectifying properties THP037 and THP056 are, however, an indication of non-ohmic contacts.

leaking p-n junction that can also contribute to the current. Ideally, the I-V curves for the p-type layers should be linear.

7 Summary

The fabrication and characterization of the broad area InP diodes needed in thermophotonic devices was investigated in this work. The original purpose was to fabricate a complete thermophotonic heat pump (THP) prototype, characterize it and possibly be able to demonstrate electroluminescent (EL) cooling.

Due to challenges met in the fabrication process of the diodes, a complete THP structure could not be fabricated but the separate diodes and their properties were studied instead, to pinpoint the origin of the leakage currents preventing the expected operation of the diodes.

In this work, 63 semiconductor samples were produced using metal-organic vapor phase epitaxy (MOVPE). All substrates were grown on an InP-substrate (either doped or intrinsic). Some samples were grown without doping to calibrate layer thickness and lattice matching, others only had one doped layer to check the doping levels and the rest were complete p-n heterojunction LEDs with varying properties.

Hall-measurements were done in the beginning of this work in order to calibrate doping concentrations. Photoluminescence (PL) measurements conclude that the samples are functional. However, the absolute value of the emission intensity could not be accurately determined due to limitations in the PL measurement setup. To produce a functional THP, it is critical that the LEDs are of high quality.

Electrical I-V measurements of the diodes revealed that the p-n junctions exhibit extremely large leakage currents and generally emitted no light under forward bias. This seems contradictive with the PL measurements where luminescence was observed and suggests that the poor performance may be related to the fabrication of the metallic contacts.

A number of reasons could be behind the large leakage currents. One could be that in the growth process, small grooves or pits are formed in the sample which extend deep into the semiconductor structure. These grooves might then be filled by the deposited contact metal and cause unwanted current paths in the diode. This would explain why PL-measurements show emission of light (before metal deposition) but the I-V curves show no light emission under forward bias and a large leakage current under reverse bias.

Atomic force microscope images were taken of sample surfaces in order to spot possible grooves or other irregularities in the substrate. Due to the small scan area of 10x10 μm nothing conclusive could however be observed from the initial measurements.

Future measurements tracking the source of the large leakage current could involve imaging with a high resolution scanning electron microscope (SEM) to detect possible surface defects and modifying the growth process. When functional diodes are fabricated, the step to fabricate and study THP prototypes should not pose insurmountable problems.

References

[1] Keyes, R. T. and Quist, T. M. Recombination radiation emitted by gallium arsenide. *Proceedings of the IRE,* 1962, vol. 50, p. 1822-1823.

[2] Oksanen, J. and Tulkki, J. Thermophotonic heat pump - a theoretical model and numerical simulations. *Journal of Applied Physics*, vol. 107, p. 093106, 2010.

[3] Oksanen, J. and Tulkki, J. Thermophotonic heat pump - towards the first demonstration of electroluminescent cooling?. *Photonics West*, San Francisco, California, USA, p. 76140F-76140F-9, 2010.

[4] Kano, K. *Semiconductor devices.* Prentice Hall, Upper Saddle River, New Jersey, 1998.

[5] Kittel, C. *Introduction to Solid State Physics,* 7th ed. New York: Wiley, 1996.

[6] Kittel, C. and Kroemer, H. *Thermal Physics,* 2nd ed. W. H. Freeman Company, 1980.

[7] Shockley, W. *Electrons and Holes in Semiconductors,* D. Van Nostrand, 1950.

[8] Schubert, E. F. *Light Emitting Diodes,* 2nd ed. Cambridge University Press, 2006.

[9] Schnitzer, I. et al. 30% external quantum efficiency from surface textured, thin-film light-emitting diodes, *Applied Physics Letters*, vol. 63, p. 2174-2176, 1993.

[10] Gauck, H. et al. External radiative quantum efficiency of 96 % from a GaAs / GaInP heterostructure, *Applied Physics A: Materials Science & Processing,* vol. 64, no. 2, p. 143-147, 1997.

[11] Born, M. and Wolf, E. *Principles of optics,* Cambridge University Press, 7th ed., 1999.

[12] Sihvola, A. and Lindell, I. *Sähkömagneettinen kenttäteoria 2. Dynaamiset kentät,* Otatieto Oy, 1996.

[13] Ordal, M. A., et al. Optical properties of the metals Al, Co, Cu, Au, Fe, Pb, Ni, Pd, Pt, Ag, Ti, and W in the infrared and far infrared. *Applied Optics,* 1983, vol. 22, no. 7.

[14] Zeman, E. J., et al. An Accurate Electromagnetic Theory Study of Surface Enhancement Factors for Ag, Au, Cu, Li, Na, Al, Ga, In, Zn and Cd. *Journal of Physical Chemistry,* 1987, vol. 91, p. 634-643.

[15] Levinshtein, IM., Rumyantsev, S. and Shur, M. *Handbook series on semiconductor parameters. Vol. 2, Ternary and quaternary III-V compounds,* World Scientific Publishing Company, 1999.

[16] Foyt, A. G. The electro-optic applications of InP. *Journal of Crystal Growth,* 1981, vol. 54, no. 1, p. 1-8.

[17] Lile, D.L. The history and future of InP based electronics and optoelectronics. *10th Intern. Conf. on Indium Phosphide and Related Materials,* 1998, p. 6-9.

[18] Stringfellow, G. B. *Organometallic Vapor-Phase Epitaxy: Theory and Practice.* Academic Press, 2nd ed., 1999.

[19] Aierken, A. Passivation of GaAs surfaces and fabrication of self-assembled In(Ga)As/GaAs quantum ring structures, Doctoral dissertation, Helsinki University of Technology, 2008.

[20] Moss, S. J and Ledwith, A. *The Chemistry of the Semiconductor Industry,* Blackie & Son Limited, Glasgow, 1987.

[21] Middleman, S. and Hochberg, A.K. *Process Engineering Analysis in Semiconductor Device Fabrication,* McGraw-Hill, p. 313, 1993.

[22] Sze, S. M. *Semiconductor Devices: Physics and Technology.* John Wiley & Sons, 1985.

[23] Coburn, J. W. and Winters, H. F. Ion- and electron-assisted gas-surface chemistry-An important effect in plasma etching. *Journal of Applied Physics,* 1979, vol. 50, p. 3189.

[24] Jansen, H., Gardeniers, H., de Boer, M., Elwenspoek, M. and Fluitman, J. A survey on the reactive ion etching of silicon in microtechnology. *J. Micromech. Microeng.,* 1996, vol. 6, p. 14-28.

[25] Franssila, S. *Introduction to microfabrication,* Wiley, 2004.

[26] Jaeger, R. C. *Introduction to Microelectronic Fabrication.* Upper Saddle River: Prentice Hall, 2002.

[27] Fewster, P. F. *X-ray Scattering from Semiconductors.* Imperial College Press, London, 2nd ed., 2001.

[28] Ventra, M., et al. *Introduction to Nanoscale Science and Technology.* Kluwer Academic Publishers, 2004.

[29] Bauer, G., Richter, W. *Optical Characterization of Epitaxial Semiconductor Layers.* Springer, Berlin, 1996.

[30] Wilson, J., et al. *Optoelectronics: An introduction.* Prentice Hall, 2nd ed., 1989.

[31] Ashcroft, N. W. and Mermin, N. D. *Solid State Physics.* HOLT, RINEHART AND WINSTON, New York, 1988.

A The e-beam evaporation process

1. Preparation:
   (a) The evaporator is kept in a modest vacuum when it is not used. The rotary and diffusion pumps are turned on.
   (b) Liquid N_2 trap is filled (N_2 cools down the system and allows faster vacuum pumping).
   (c) The samples are attached to the sample holders with the n-side exposed.
   (d) Air is admitted to the chamber and the samples and metals to be evaporated are inserted into the chamber.
   (e) Rough pumping for 5-10 min.
   (f) When the pressure < 0.2 mbar fine pumping is begun.
   (g) Approx. 3 h waiting for the pressure to reach 2×10^{-6} mbar.
2. Thermal evaporation of 5 nm Au:
   (a) The current through Au is set to 60-80 A.
   (b) Samples are placed in the line of evaporation.
   (c) Au evaporates at ~ 1 nm/s for 5 s.
   (d) Current turned off.
3. E-beam evaporation of 10 nm Ni:
   (a) The e-beam voltage is set to ~ 3.2 kV.
   (b) The filament current is set to ~ 300 mA.
   (c) Ni evaporates at 1 nm/s for 100 s to clean the Ni crucible.
   (d) Samples are placed in the line of evaporation and evaporation at 1 nm/s for 10 s.
   (e) Filament current and voltage are set to 0.
4. Thermal evaporation of 70 nm Au:
   (a) Phase 2 repeated.
   (b) All the remaining gold is evaporated.
5. Preparation for p-side evaporation
   (a) Air is admitted to the chamber and the samples and metals are removed.
   (b) Samples are attached to the sample holder with p-side exposed.
   (c) Samples and metals are inserted.

   (d) Rough pumping for $\approx$ 10 min.

   (e) When the pressure $<$ 0.2 mbar fine pumping is begun.

   (f) Approx. 1.5 h waiting for the pressure to reach 2×10^{-6} mbar.

6. Thermal evaporation of 5 nm Au:

   (a) Phase 2 repeated.

7. E-beam evaporation of 10 nm Ti:

   (a) Phase 3 repeated with Ti.

8. Thermal evaporation of 70 nm Au:

   (a) Phase 2 repeated.

   (b) All the remaining gold is evaporated.

9. Finishing:

   (a) Air is admitted to the chamber and the samples and metals are removed.

   (b) Chamber is closed and rough pumping is made for 5-10 min.

   (c) Rotary and diffusion pumps are turned off and the chamber is left in a modest vacuum.